



# Effect of compressibility factor on the hydrodynamics of naphtha catalytic-reforming reactors

Aminu Zakari Yusuf<sup>1,2</sup> · Yakubu Mandafiya John<sup>1</sup> · Benjamin Olufemi Aderemi<sup>3</sup> · Raj Patel<sup>1</sup> · Iqbal M. Mujtaba<sup>1</sup>

Received: 4 April 2019 / Accepted: 1 July 2019 / Published online: 16 July 2019  
© The Author(s) 2019

## Abstract

A detailed steady-state catalytic-reforming unit (CRU) reactor process model is simulated in this work, and for the first time, different compressibility  $Z$  factor correlations have been applied using gPROMS software. The CRU has been modeled and simulated with the assumption that the gas phase behaves like an ideal gas. This is assumed for the four reactors in series and for different conditions of hydrogen–hydrocarbon ratio (HHR), operating temperature, and pressure. The results show that the  $Z$  factor varies at every point along the height of the reactors depending on reaction operating pressure, temperature, and HHR ratio. It also shows that the magnitude of deviation from ideal gas behaviour can be measured over the reactor height. The  $Z$  factor correlation of Mahmoud (J Energy Resour Technol Trans ASME 136:012903, 2014) is found to be suitable for predicting the  $Z$  factor distribution in the reactors.

**Keywords** Catalytic reforming unit · Hydrogen–Hydrocarbon ratio · Compressibility factor · Naphtha · Fluid bed reactor

## Abbreviations

$a, b, c$	Parameters from hydrogen reaction rate equation	$F$	Molar flow (kmol/h)
$P$	Paraffins	$g_c$	Force to mass conversion factor, $9.8066 \text{ (kg}_m \text{ m)/(kg}_f \text{ s}^2)$
$N$	Naphthenes	$G$	Mass velocity ( $\text{kg/m}^2 \text{ h}$ )
$A$	Aromatics	$\Delta G^\circ$	Reaction standard Gibbs energy (kJ/kmol k)
$A, B, C, D$	Constants for calculating heat capacities	$\Delta H$	Heat of reaction (kJ/kmol k)
$Aa, Bb, Cc, Dd, Ee$	Constants for calculating research octane number (RON)	$k_i$	Kinetic constant at $T$ (kmol/h)
$A_{10}$	Aromatics having ten atoms of carbon	$k_i^\circ$	Kinetic constant at $T$ (kmol/h)
$N_{10}$	Naphthenes having ten atoms of carbon	$k_e$	Equilibrium constant
$P_{10}$	Paraffins having ten atoms of carbon	WHSV	Weight hourly space velocity ( $\text{h}^{-1}$ )
$C_p$	Heat capacity (kJ/kmol k)	$MW$	Molecular weight (g/gmol)
$d_p$	Particle diameter (m)	$n$	Reaction order
$E_A$	Activation energy (kJ/kmol)	$N$	Number of reactions naphthenes
		NC	Number of components
		$P_i$	Partial pressure of component $i$ (Pa)
		$P$	Pressure (Pa)
		$P_o$	Standard base pressure (Pa)
		$r_i$	Rate of reaction of component $i$ (kmol/h)
		$R_g$	Universal constant of gases (kJ/mol k)
		$A$	Cross sectional area ( $\text{m}^2$ )
		SV	Space velocity ( $\text{h}^{-1}$ )
		$T$	Reaction temperature (K)
		$T_o$	Base reaction temperature (K)
		$y_i$	Molar composition of component $i$ (mol%)
		$z$	Reactor height (m)

✉ Iqbal M. Mujtaba  
I.M.Mujtaba@bradford.ac.uk

<sup>1</sup> Chemical Engineering Department, Faculty of Engineering and Informatics, University of Bradford, Bradford BD7 1DP, UK

<sup>2</sup> Nigerian National Petroleum Cooperation (NNPC), Abuja, Nigeria

<sup>3</sup> Chemical Engineering Department, Ahmadu Bello University, Zaria, Nigeria

### Greek letters

$\varepsilon$	Void fraction of catalyst bed
$\rho$	Density of gas mixture
$\rho_c$	Density of catalyst
$\mu$	Viscosity of gas mixture

## Introduction

The catalytic-reforming unit is an important integral part of the refinery operations. It is used to improve the quality of low-to-high-octane naphtha in a series of reactors (three or four, depending on the design of the refinery). The system can either be a semi regenerative (fixed bed) where the reaction proceeds for a particular period and the catalyst is regenerated, or a continuous one where the catalyst is continuously regenerated in a regenerator. The continuous process has the advantage of using a lower pressure and lower hydrogen usage. However, there is the need for more technical monitoring for the mechanisms of engagement and disengagement of the catalyst from the last reactor through the regenerator and back to the first reactor in continuous flow. To improve the quality and the yield of the reformat, one important aspect is the hydrodynamics study of the reaction which helps to improve the efficiency of the system by maintaining an effective pressure gradient across the reactors. The low octane naphtha meets recycled hydrogen from the recycle gas compressor and enters the first heater that precedes the reactor, a process that continues for the other four reactors and heaters in series. The hydrodynamics is important, since the variations of temperature and pressure of the reaction affect the rate of reactions, which in turn affect the entire system responses. Increase in reaction pressure decreases the reformat yield, the hydrogen yield, and the research octane number, RON [10]. The Ergun equation, as a function of density, viscosity, bed void, particle diameter, and mass flux, is used to model the behaviour of pressure in these reactors. Since these reactions' parameters such as enthalpy, density, viscosity, and pressure change with reactor height, there is need to study the effect of the compressibility factor which affects these parameters [13]. In the past, all the CRU was modeled with compressibility factor  $Z$  as unity, implying an ideal gas system, which may not always be the case. Real systems tend to vary from ideal system. The  $Z$  factor of a fluid catalytic cracking (FCC) riser has been modeled as unity until John et al. [13] simulated the riser with different  $Z$  factor correlations and found that the riser can be modeled with Heidaryan et al. [11] correlation. Hence, the need to find the actual  $Z$  factor for the CRU and consequently investigate the response of the CRU under real system conditions.

In characterizing fluid flow behaviour in the oil and gas, it is very important to study the effect of  $Z$  factor, both upstream and downstream [12]. The fluid can be said to be

compressible or incompressible depending on the type of process which it undergoes [11]. Variation in density of the gas during reaction, as in the case with catalytic-reforming, may bring about change in compressibility factor. Therefore, assuming a changing gas density system as ideal may not be always true especially when there is velocity variation as the gas density varies and the fluid could be compressible [5]. Transport and physical properties like density, viscosity, and fraction of void of the treated naphtha during reaction could change when reaction conditions [temperature, pressure, feed rate, and hydrogen–hydrocarbon ratio (HHR)] are altered. Since there is significant variation of these properties with operating conditions, there is a need to study the compressibility factor effect. An important variable in the process conditions is the HHR which preserves the catalyst activity by sweeping off amorphous carbon deposit on the catalyst, but has little effect on the aromatics and reformat yield. This variable has an effect on the reactor pressure, since it increases the partial pressure of the vapor by increasing the number of moles of hydrogen; hence, it will have effect on the reaction hydrodynamics. To have optimum and precise condition of the catalyst, the reactor bed and other equipment should adhere to professional design of the catalytic-reforming plant. In this paper, the effect of compressibility factor on reaction pressure, which is a major hydrodynamic parameter, is studied. This will help in determining an appropriate gas compressibility factor to be applied in plant design and when any modifications of the design are required such as scale up or scale down, the assumption of ideal case may not always hold. The precise compressibility factor can assist to predict accurately the hydrodynamic behaviour of operational variables like pressure drop across the reactors to ensure effective process plant design.

In this work, the effect of compressibility factor on four commercial catalytic naphtha reactors in series is investigated for the first time, by applying various correlations to model the behaviour of the reaction using gPROMS software. Hence, the  $Z$  factor variation across the reactors heights will be determined for different  $Z$  factors and a suitable correlation model for the CRU will be determined.

## Compressibility factor $Z$

The compressibility factor of gases ( $Z$  factor) from principle of corresponding of state is defined based on the pseudo-reduced temperature ( $T_{pr}$ ) and pseudo-reduced pressure ( $P_{pr}$ ), which are important thermodynamic variables when determining the behaviour of gases and liquids both in upstream and downstream computations [11]. These are described in Eqs. (2) and (3):

$$PV = ZnRT, \quad (1)$$

$$T_{pr} = \frac{T}{T_c}, \tag{2}$$

$$P_{pr} = \frac{P}{P_c}. \tag{3}$$

The three equations are applied to both real and ideal gases where the Z factor is unity for ideal cases which in reality is non-existent. It is thus of paramount importance to predict the compressibility effect in gaseous phase reactions when dealing with changes of physical and transport properties. The simple definition is the ratio of actual gas volume to the gas volume of ideal gas implying a measure and extent of deviation from ideal behaviour [12].

According to Fayazi et al. [9], this parameter can be determined experimentally or from equations of state or using semi-empirical correlations. The use of experimental data seems more expensive and takes a lot of time and energy and that could be so tedious considering the number of gases in petroleum to account for Ahmed [1], whilst the use of semi-empirical correlations has proved accurate and simpler than even the use of equations of state EoS [8]. Whenever the pseudo-reduced pressure and pseudo-reduced temperature of the gas is known, the Z factor of the vapor of the hydrocarbon could be predicted and estimated [9].

In this work,  $T_{pr}$  and  $P_{pr}$  are computed using Eqs. (2) and (3). The  $T_{pr}$  and  $P_{pr}$  are shown in Fig. 1 with variation along the reactor heights. The  $P_{pr}$  obtained is in the range  $1.218066 \leq P_{pr} \leq 1.023427$  and its  $T_{pr}$  is within the range  $0.528144 \leq T_{pr} \leq 0.348992$ . The values of the  $T_{pr}$  and  $P_{pr}$

may change based on the conditions of operations of the reaction. This implies that, as the variables of the process which affect the temperature and pressure of the CRU vary during plant run, the  $T_{pr}$  and  $P_{pr}$  will also vary. Conversely, the compressibility, a function of  $T_{pr}$  and  $P_{pr}$  will as well not remain constant but change.

There are some common empirical correlations [6, 14] that are not suitable when  $T_{pr} \leq 0.92$ . Some of the correlations applied in this research accept  $T_{pr}$  above 0.92 [11, 17]. In the quest to determine the most accurate and precise Z factor for the vapor state of the reactions, a number of different empirical correlations are used. Each of the Z factors determined is compared with both the plant data and that of the literature and ascertain which of the compressibility factors predicts closely. The computed pseudo-reduced temperature here is outside the boundary of some of the empirical correlations used, but the  $P_{pr}$  is within the range  $0.364 \leq P_{pr} \leq 0.375$  which lies within the boundaries of the  $P_{pr}$  in the used empirical correlations in this work which are given below.

1. Azizi et al. [3] Z factor:

Azizi et al. [3] established their Z factor empirical correlation by applying standing Katz chart with about 3038 points with a range of  $P_{pr}$  of  $0.2 \leq P_{pr} \leq 11$  and  $T_{pr}$  range of  $1.1 \leq T_{pr} \leq 2$ . This is presented in Eq. (4):

$$Z = A + \frac{B + C}{D + E}. \tag{4}$$

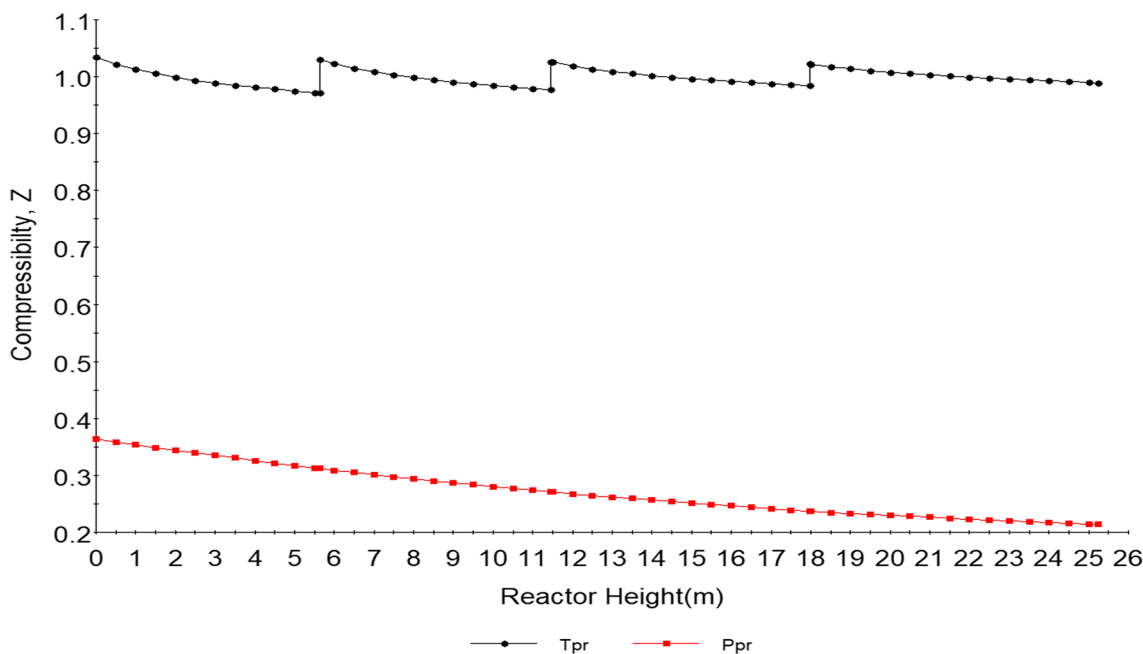


Fig. 1 Variation of  $P_{pr}$  and  $T_{pr}$  along reactor heights

The variables in Eq. (4) are presented in Eqs. (5–9):

$$A = aT_{pr}^{2.16} + bP_{pr}^{1.028} + cP_{pr}^{1.58}T_{pr}^{-2.1} + d \ln T_{pr}^{-0.5}, \tag{5}$$

$$B = e + fT_{pr}^{2.4} + gP_{pr}^{1.56} + hP_{pr}^{0.124}T_{pr}^{3.033}, \tag{6}$$

$$C = i \ln T_{pr}^{-1.28} + j \ln T_{pr}^{1.37} + k \ln(P_{pr}) + l \ln(P_{pr})^2 + m \ln(P_{pr}) \ln(T_{pr}), \tag{7}$$

$$D = 1 + nT_{pr}^{5.55} + oP_{pr}^{0.68}T_{pr}^{0.33}, \tag{8}$$

$$E = p \ln T_{pr}^{1.18} + q \ln T_{pr}^{2.1} + r \ln(P_{pr}) + s \ln(P_{pr})^2 + t \ln(P_{pr}) \ln(T_{pr}). \tag{9}$$

The tuned coefficients for Eqs. (5–9) are presented in Appendix Table 14.

2. Bahadori et al. [4] compressibility factor:

Compressibility factor of Bahadori et al. [4] is given in Eq. (10) and its coefficients are presented in Eqs. (10–14) [4]. The range is  $0.2 \leq P_{pr} \leq 16$  and  $1.05 \leq T_{pr} \leq 2.4$ :

$$Z = a - bP_{pr} + cP_{pr}^2 + dP_{pr}^3, \tag{10}$$

$$a = Aa + BaT_{pr} + CaT_{pr}^2 + DaT_{pr}^3, \tag{11}$$

$$b = Ab + BbT_{pr} + CbT_{pr}^2 + DbT_{pr}^3, \tag{12}$$

$$c = Ac + BcT_{pr} + CcT_{pr}^2 + DcT_{pr}^3, \tag{13}$$

$$d = Ad + BdT_{pr} + CdT_{pr}^2 + DdT_{pr}^3. \tag{14}$$

The tuned coefficients for Eqs. (10–14) are presented in Appendix Table 15.

3. Compressibility factor Heidaryan et al. [11]:

The compressibility factor for Heidaryan et al. [11] is defined as in Eq. (15) and the fine-tuned coefficients are given in Appendix Table 16. The  $P_{pr}$  is within  $0.2 \leq P_{pr} \leq 3$  and this is within the range of that of Heidaryan et al. [12]:

$$Z = \ln \left[ \frac{A_1 + A_3 \ln(P_{pr}) + \frac{A_5}{T_{pr}} + A_7(\ln P_{pr})^2 + \frac{A_9}{T_{pr}^2} + \frac{A_{11}}{T_{pr}} \ln(P_{pr})}{1 + A_2 \ln(P_{pr}) + \frac{A_4}{T_{pr}} + A_6(\ln P_{pr})^2 + \frac{A_8}{T_{pr}^2} + \frac{A_{10}}{T_{pr}} \ln(P_{pr})} \right]. \tag{15}$$

4. Heidaryan et al. [12] compressibility factor:

The compressibility factor of Heidaryan et al. [11, 12] is defined in Eq. (16) with the tuned coefficients reported in Appendix Table 17. The boundaries of the  $P_{pr}$  and  $T_{pr}$  are  $0.20 \leq P_{pr} \leq 15.0$  and  $1.20 \leq T_{pr} \leq 3.0$  (Heidaryan et al. 2010c). The boundary of the  $P_{pr}$  here in this research is concurrent as that of Heidaryan et al. [11]:

$$Z = \frac{A_1 + A_2 \ln(P_{pr}) + A_3(\ln P_{pr})^2 + A_4(\ln P_{pr})^3 + \frac{A_5}{T_{pr}} + \frac{A_6}{T_{pr}^2}}{1 + A_7 \ln(P_{pr}) + A_8(\ln P_{pr})^2 + \frac{A_9}{T_{pr}} + \frac{A_{10}}{T_{pr}^2}}. \tag{16}$$

5. Mahmoud [16] compressibility Z factor:

The compressibility Z factor for Mahmoud [16] is defined by Eq. (17). The correlation was derived from measurements taken of 300 Z factors [16]:

$$Z = (0.702e^{(-2.5T_{pr})}P_{pr}^2 - (5.524e^{(-2.5T_{pr})})P_{pr} + (0.044T_{pr}^2 + 1.15)). \tag{17}$$

6. Papay [17] compressibility factor:

The compressibility factor Z of Papay [17] is defined by Eq. (18) [15]:

$$Z = 1 - \frac{P_{pr}}{T_{pr}} \left[ 0.3648758 - 0.04188423 \left( \frac{P_{pr}}{T_{pr}} \right) \right]. \tag{18}$$

7. Z factor correlation of Sanjari and Lay [20]:

Sanjari and Lay [17] got their compressibility factor correlation from 5844 experimental data points of different compressibility factors within the boundary of  $0.010 \leq P_{pr} \leq 15.0$  and  $1.0 \leq T_{pr} \leq 3.0$ . It is reported in Eq. (19) with the fine-tuned coefficients given from Appendix Table 18:

$$Z = 1.0 + A_1P_{pr} + A_2(P_{pr})^2 + \frac{A_3P_{pr}^{A_4}}{T_{pr}^{A_5}} + \frac{A_6P_{pr}^{(A_4+1)}}{T_{pr}^{A_7}} + \frac{A_8P_{pr}^{(A_4+2)}}{T_{pr}^{(A_7+1)}}. \tag{19}$$

8. Shokir et al. [21] Z factor:

The Shokir et al. [21] compressibility factor is defined by Eq. (20), with its parameters given in Eqs. (21–25) [21]:

$$Z = A + B + C + D + E, \tag{20}$$

$$A = 2.679562 \frac{(2T_{pr} - P_{pr} - 1)}{[(P_{pr}^2 + T_{pr}^3)/P_{pr}]}, \tag{21}$$

$$B = -7.686825 \left[ \frac{(P_{pr}T_{pr} + P_{pr}^2)}{[(P_{pr}T_{pr} + 2T_{pr}^2 + T_{pr}^3)]} \right], \tag{22}$$

$$C = -0.000624(P_{pr}T_{pr}^2 - T_{pr}P_{pr}^2 + T_{pr}P_{pr}^3 + 2P_{pr}T_{pr} - 2P_{pr}^2 + 2P_{pr}^3), \tag{23}$$

$$D = 3.067747 \frac{(T_{pr} - P_{pr})}{[(P_{pr}^2 + T_{pr} + P_{pr})]}, \tag{24}$$

$$E = \frac{0.068059}{P_{pr}T_{pr}} + 0.139489T_{pr}^2 - 0.081873P_{pr}^2 - \left[ \frac{0.041098T_{pr}}{P_{pr}} \right] + \left[ \frac{8.152325P_{pr}}{T_{pr}} \right] - 1.63028P_{pr} + 0.24287T_{pr} - 2.64988. \tag{25}$$

### Kinetic models

The assumptions made, model equations used, and the method and procedures are presented in this section. The reactors are in series, as shown in Fig. 2. The first reactor is 5.632 m in height, 5.83 m for the second, 6.51 m for the third, and 7.26 m for the fourth reactors. The total height of the reactors in series is 25.232 m.

Some of the assumptions made are as follows:

- The reactors are modeled as adiabatic processes, i.e., no heat escapes or enters the reactors due to sufficient lagging.
- The reactors are modeled as plug flow, because naphtha flows as gas through the reactor at the pressure and temperature of reaction. Due to the reactor length, dispersion of matter is negligible as supported by a criterion reported elsewhere [10].

- The reaction is considered as first order, because the reforming reaction uses HHR higher than the hydrocarbon concentration. Hence, its concentration is grouped with reaction coefficient.
- Pseudo-homogeneous reactor model is assumed, since the vapor phase reaction is too complex to solve heterogeneously and the diffusion along the radius is negligible with the height of the reactor much greater than the radius.

Various models have been developed for both steady-state and dynamic processes of the catalytic-reforming reaction with different lumps to investigate the behaviour of the reaction and product distribution. The reaction steps and equations of the model are shown in Table 1 (a zero value is registered when the data are not available).

The kinetic rate equations for the components are given in Eqs. (26–50) where SV is space velocity and  $\frac{1}{SV}$  is residence time:

$$\begin{aligned} \frac{dP_1}{d(1/SV)} = & K_2P_{11} + K_8P_{10} + K_{14}P_9 + K_{19}P_8 + K_{24}P_7 \\ & + K_{29}P_6 + K_{32}P_5 + K_{36}N_{11} \\ & + K_{41}N_{10} + K_{45}N_9 + K_{50}N_8 + K_{50}A_{11} + K_{62}A_{10} \\ & + K_{66}A_9 + K_{99}A_8, \end{aligned} \tag{26}$$

$$\begin{aligned} \frac{dP_2}{d(1/SV)} = & K_3P_{11} + K_9P_{10} + K_{15}P_9 + K_{20}P_8 + K_{25}P_7 + K_{30}P_6 \\ & + K_{33}P_5 + K_{37}N_{11} + K_{42}N_{30} + K_{47}N_9 \\ & + K_{60}A_{11} + K_{62}A_{10} + K_{67}A_9, \end{aligned} \tag{27}$$

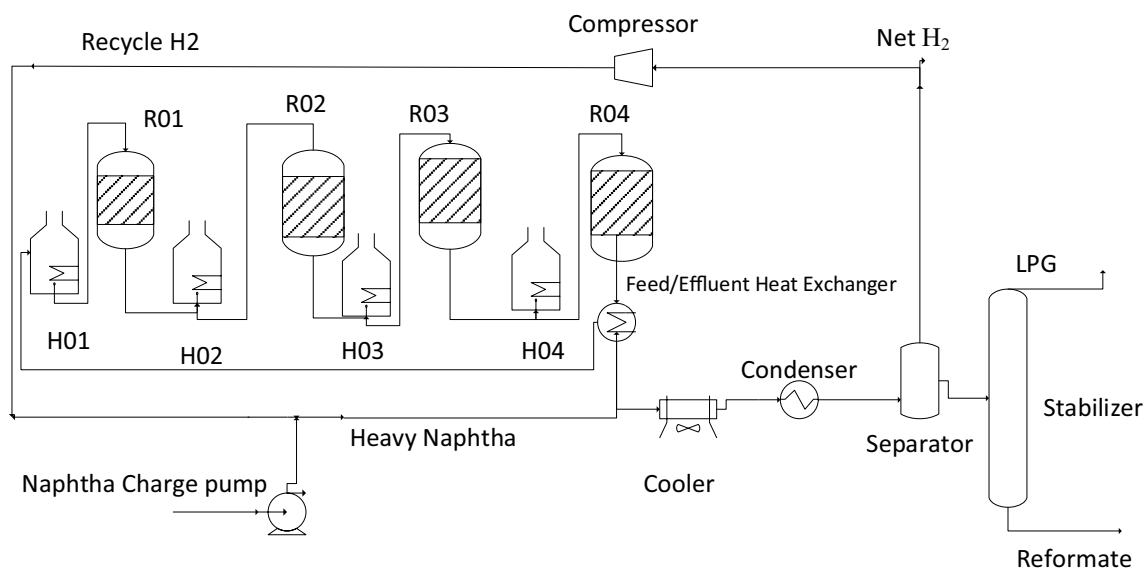


Fig. 2 Catalytic-reforming process with four reactors in series

**Table 1** Table of reaction steps and rate constants of the model (adapted from Elizalde et al. [7])

Reaction steps of the reactions	Rate constants (kg/h kg) <sup>-1</sup>	
<i>Dehydrogenation reactions of paraffins (P) to naphthenes (N)</i>		
1. $P_{11} \rightarrow N_{11} + H_2$	0.00	$k_1$
2. $P_{10} \rightarrow N_{10} + H_2$	2.54	$k_7$
3. $P_9 \rightarrow N_9 + H_2$	1.81	$k_{13}$
4. $P_8 \rightarrow N_8 + H_2$	1.33	$k_{18}$
5. $P_7 \rightarrow N_7 + H_2$	0.58	$k_{23}$
6. $P_6 \rightarrow N_6 + H_2$	0.00	$k_{27}$
7. $P_6 \rightarrow MCP + H_2$	0.00	$k_{28}$
<i>Hydrocracking reactions of paraffins (P)</i>		
8. $P_{11} + H_2 \rightarrow P_{10} + P_1$	0.00	$k_2$
9. $P_{11} + H_2 \rightarrow P_9 + P_2$	0.00	$k_3$
10. $P_{11} + H_2 \rightarrow P_8 + P_3$	0.00	$k_4$
11. $P_{11} + H_2 \rightarrow P_7 + P_4$	0.00	$k_5$
12. $P_{11} + H_2 \rightarrow P_6 + P_5$	0.00	$k_6$
13. $P_{10} + H_2 \rightarrow P_9 + P_1$	0.49	$k_8$
14. $P_{11} + H_2 \rightarrow P_8 + P_2$	0.63	$k_9$
15. $P_{10} + H_2 \rightarrow P_7 + P_3$	1.09	$k_{10}$
16. $P_{10} + H_2 \rightarrow P_6 + P_4$	0.89	$k_{11}$
17. $P_{10} + H_2 \rightarrow 2P_5$	1.24	$k_{12}$
18. $P_9 + H_2 \rightarrow P_8 + P_1$	0.30	$k_{14}$
19. $P_9 + H_2 \rightarrow P_7 + P_2$	0.39	$k_{15}$
20. $P_9 + H_2 \rightarrow P_6 + P_3$	0.68	$k_{16}$
21. $P_9 + H_2 \rightarrow P_5 + P_4$	0.55	$k_{17}$
22. $P_8 + H_2 \rightarrow P_7 + P_1$	0.19	$k_{19}$
23. $P_8 + H_2 \rightarrow P_6 + P_2$	0.25	$k_{20}$
24. $P_8 + H_2 \rightarrow P_5 + P_3$	0.43	$k_{21}$
25. $P_8 + H_2 \rightarrow 2P_4$	0.35	$k_{22}$
26. $P_7 + H_2 \rightarrow P_6 + P_1$	0.14	$k_{24}$
27. $P_7 + H_2 \rightarrow P_5 + P_2$	0.18	$k_{25}$
28. $P_7 + H_2 \rightarrow P_4 + P_3$	0.32	$k_{26}$
29. $P_6 + H_2 \rightarrow P_5 + P_1$	0.14	$k_{27}$
30. $P_6 + H_2 \rightarrow P_4 + P_2$	0.18	$k_{29}$
31. $P_6 + H_2 \rightarrow 2P_3$	0.27	$k_{31}$
32. $P_5 + H_2 \rightarrow P_4 + P_1$	0.12	$k_{32}$
33. $P_5 + H_2 \rightarrow P_3 + P_2$	0.15	$k_{33}$
<i>Dehydrogenation reactions of naphthenes (N)</i>		
34. $N_{11} \rightarrow A_{11} + 3H_2$	0.00	$k_{35}$
35. $N_{10} \rightarrow A_{10} + 3H_2$	24.5	$k_{40}$
36. $N_9 \rightarrow A_9 + 3H_2$	24.5	$k_{44}$
37. $N_8 \rightarrow A_8 + 3H_2$	21.5	$k_{49}$
38. $N_7 \rightarrow A_7 + 3H_2$	9.03	$k_{52}$
39. $N_6 \rightarrow A_6 + 3H_2$	4.02	$k_{54}$
40. $N_{11} + H_2 \rightarrow P_{11}$	0.00	$k_{34}$
41. $N_{10} + H_2 \rightarrow P_{10}$	0.54	$k_{39}$
42. $N_9 + H_2 \rightarrow P_9$	0.54	$k_{44}$
43. $N_8 + H_2 \rightarrow P_8$	0.47	$k_{48}$
44. $N_7 + H_2 \rightarrow P_7$	0.20	$k_{51}$

**Table 1** (continued)

Reaction steps of the reactions	Rate constants (kg/h kg) <sup>-1</sup>	
45. $N_6 + H_2 \rightarrow P_6$	1.48	$k_{53}$
46. $N_6 \rightarrow MCP$	0.00	$k_{55}$
47. $MCP + H_2 \rightarrow P_6$	0.00	$k_{56}$
48. $MCP \rightarrow N_6$	0.00	$k_{57}$
<i>Hydrocracking reactions of naphthenes (N)</i>		
49. $N_{11} + H_2 \rightarrow N_{10} + P_1$	0.00	$k_{36}$
50. $N_{11} + H_2 \rightarrow N_9 + P_2$	0.00	$k_{37}$
51. $N_{11} + H_2 \rightarrow N_8 + P_3$	0.00	$k_{38}$
52. $N_{10} + H_2 \rightarrow N_9 + P_1$	1.84	$k_{41}$
53. $N_{10} + H_2 \rightarrow N_8 + P_2$	1.34	$k_{42}$
54. $N_{10} + H_2 \rightarrow N_7 + P_3$	0.80	$k_{43}$
55. $N_9 + H_2 \rightarrow N_8 + P_1$	1.27	$k_{45}$
56. $N_9 + H_2 \rightarrow N_7 + P_2$	1.27	$k_{46}$
57. $N_8 + H_2 \rightarrow N_7 + P_1$	0.09	$k_{47}$
<i>Hydrodealkylation reactions of aromatics (A)</i>		
58. $A_{11} + H_2 \rightarrow A_{10} + P_1$	0.00	$k_{59}$
59. $A_{11} + H_2 \rightarrow A_9 + P_2$	0.00	$k_{60}$
60. $A_{10} + H_2 \rightarrow A_9 + P_1$	0.06	$k_{62}$
61. $A_{10} + H_2 \rightarrow A_8 + P_2$	0.06	$k_{63}$
62. $A_{10} + H_2 \rightarrow A_7 + P_3$	0.00	$k_{64}$
63. $A_9 + H_2 \rightarrow A_8 + P_1$	0.05	$k_{66}$
64. $A_9 + H_2 \rightarrow A_7 + P_2$	0.05	$k_{67}$
65. $A_8 + H_2 \rightarrow A_7 + P_1$	0.01	$k_{69}$
66. $A_{11} + 4H_2 \rightarrow P_{11}$	0.00	$k_{58}$
67. $A_{10} + 4H_2 \rightarrow P_{10}$	0.00	$k_{61}$
68. $A_9 + 4H_2 \rightarrow P_9$	0.16	$k_{65}$
69. $A_8 + 4H_2 \rightarrow P_8$	0.16	$k_{68}$
70. $A_7 + 4H_2 \rightarrow P_7$	0.16	$k_{70}$
71. $A_6 + 3H_2 \rightarrow N_6$	0.45	$k_{71}$

$$\frac{dP_3}{d(1/SV)} = K_4 P_{11} + K_{10} P_{10} + K_{16} P_9 + K_{21} P_8 + K_{26} P_7 + 2K_{31} P_6 + K_{33} P_5 + K_{38} N_{11} + K_{43} N_{10} + K_{64} A_{10}, \quad (28)$$

$$\frac{dP_4}{d(1/SV)} = K_5 P_{11} + K_{11} P_{10} + K_{17} P_9 + 2K_{22} P_8 + K_{25} P_7 + K_{10} P_6 + K_{32} P_5, \quad (29)$$

$$\frac{dP_5}{d(1/SV)} = K_6 P_{11} + 2K_{12} P_{10} + K_{17} P_{19} + K_{21} P_8 + K_{24} P_7 + K_{29} P_6 + (K_{32} + K_{33}) P_5, \quad (30)$$



$$\begin{aligned} \frac{dP_6}{d(1/SV)} &= K_6P_{11} + K_{11}P_{10} + K_{16}P_9 + K_{20}P_8 \\ &+ K_{25}P_7 + K_{53}N_6 + K_{96}MPC \\ &- (K_{27} + K_{28} + K_{29} + K_{30} + K_{31})P_6, \end{aligned} \tag{31}$$

$$\begin{aligned} \frac{dP_7}{d(1/SV)} &= K_5P_{11} + K_{10}P_{10} + K_{15}P_9 + K_{19}P_8 + K_{51}N_7 + K_{70}A_7 \\ &- (K_{23} + K_{24} + K_{25} + K_{26} + K_{27})P_7, \end{aligned} \tag{32}$$

$$\begin{aligned} \frac{dP_8}{d(1/SV)} &= K_4P_{11} + K_9P_{10} + K_{14}P_9 + K_{48}N_8 + K_{68}A_8 \\ &- (K_{18} + K_{19} + K_{20} + K_{21} + K_{22})P_8, \end{aligned} \tag{33}$$

$$\begin{aligned} \frac{dP_9}{d(1/SV)} &= K_3P_{11} + K_8P_{10} + K_{44}N_9 + K_{66}A_9 \\ &- (K_{13} + K_{14} + K_{15} + K_{16} + K_{17})P_9, \end{aligned} \tag{34}$$

$$\begin{aligned} \frac{dP_{10}}{d(1/SV)} &= K_2P_{11} + K_{39}N_{10} + K_{61}A_{10} \\ &- (K_7 + K_8 + K_9 + K_{10} + K_{11} + K_{12})P_{10}, \end{aligned} \tag{35}$$

$$\begin{aligned} \frac{dP_{11}}{d(1/SV)} &= K_{34}N_{11} + K_{58}A_{11} - (K_1 + K_2 + K_3 + K_4 + K_5 + K_6)P_1, \end{aligned} \tag{36}$$

$$\begin{aligned} \frac{dMCP}{d(1/SV)} &= K_{28}P_6 + K_{55}N_6 - (K_{56} + K_{57}), \end{aligned} \tag{37}$$

$$\begin{aligned} \frac{dN_6}{d(1/SV)} &= K_{27}P_6 + K_{57}MCP + K_{71}A_6 - (K_{53} + K_{54} + K_{55})N_6, \end{aligned} \tag{38}$$

$$\begin{aligned} \frac{dN_7}{d(1/SV)} &= K_{23}P_7 + K_{43}N_{10} + K_{47}N_{10} + K_{50}N_9 - (K_{51} + K_{52})N_7, \end{aligned} \tag{39}$$

$$\begin{aligned} \frac{dN_8}{d(1/SV)} &= K_{18}P_8 + K_{38}N_{11} + K_{42}N_{10} + K_{46}N_9 - (K_{48} + K_{49} + K_{50})N_8, \end{aligned} \tag{40}$$

$$\begin{aligned} \frac{dN_9}{d(1/SV)} &= K_{13}P_9 + K_{37}N_{11} + K_{41}N_{10} - (K_{44} + K_{45} + K_{46} + K_{47})N_9, \end{aligned} \tag{41}$$

$$\begin{aligned} \frac{dN_{10}}{d(1/SV)} &= K_7P_{10} + K_{36}N_{11} - (K_{39} + K_{40} + K_{41} + K_{42} + K_{43})N_{10}, \end{aligned} \tag{42}$$

$$\begin{aligned} \frac{dN_{11}}{d(1/SV)} &= K_1P_{11} - (K_{34} + K_{35} + K_{36} + K_{37} + K_{38})N_{11}, \end{aligned} \tag{43}$$

$$\begin{aligned} \frac{dA_6}{d(1/SV)} &= K_{49}N_8 + K_{63}A_{10} + K_{66}A_{10} - (K_{68} + K_{69})A_8, \end{aligned} \tag{44}$$

$$\begin{aligned} \frac{dA_7}{d(1/SV)} &= K_{49}N_8 + K_{63}A_{10} + K_{66}A_{10} - (K_{68} + K_{69})A_8, \end{aligned} \tag{45}$$

$$\begin{aligned} \frac{dA_8}{d(1/SV)} &= K_{49}N_8 + K_{63}A_{10} + K_{66}A_{10} - (K_{68} + K_{69})A_8, \end{aligned} \tag{46}$$

$$\begin{aligned} \frac{dA_9}{d(1/SV)} &= K_{45}N_9 + K_{60}A_{11} + K_{62}A_{10} - (K_{65} + K_{66} + K_{67})A_9, \end{aligned} \tag{47}$$

$$\begin{aligned} \frac{dA_{10}}{d(1/SV)} &= K_{40}N_{10} + K_{59}A_{11} - (K_{61} + K_{62} + K_{63} + K_{64})A_{10}, \end{aligned} \tag{48}$$

$$\begin{aligned} \frac{dA_{11}}{d(1/SV)} &= K_{35}N_{11} - (K_{58} + K_{59} + K_{60})A_{11}, \end{aligned} \tag{49}$$

$$\begin{aligned} \frac{dH_2}{d(1/SV)} &= a_1P_{11} + a_2P_{10} + a_3P_9 + a_4P_8 \\ &+ a_5P_7 + a_6P_6 + a_7P_5 + b_1N_{11} + b_2N_{10} + b_3N_9 \\ &+ b_4N_8 + b_5N_7 + b_6N_6 + c_1A_{11} + c_2A_{10} \\ &+ c_3A_9 + c_4A_8 + c_5A_7 + c_6A_6, \end{aligned} \tag{50}$$

$$K_i = K_i^0 \left[ \frac{E_{Ai}}{R} \left( \frac{1}{T_0} - \frac{1}{T} \right) \right] \left( \frac{P}{P_0} \right)^{a_k}, \tag{51}$$

where  $K_i$  is the kinetic constants for the reactions,  $T_0$  and  $P_0$  are the reference temperatures and pressures,  $E_{Ai}$  the activation energy, and  $w$  is an exponential effect of pressure, as given in Tables 2 and 3, respectively.  $k_i$ ,  $E_{Ai}$ ,  $w$ ,  $T_0$ , and  $P_0$  are values obtained from Elizalde and Ancheyta [7].

**Table 2** Activation energies for the reactions (adapted from Elizalde and Ancheyta [7])

Reaction	$E_a$ (kcal/mol)
Dehydrocyclization of paraffins ( $P_n \rightarrow N_n$ )	45
Hydrocracking of paraffins ( $P_n \rightarrow P_{n-i} + P_i$ )	55
Dehydrogenation of naphthenes ( $N_n \rightarrow A_n$ )	30
Hydrodealkylation of naphthenes ( $N_n \rightarrow N_{n-i} + P_i$ )	55
Ring opening of naphthenes ( $N_n \rightarrow P_n$ )	45
Hydrodealkylation of aromatics ( $A_n \rightarrow A_{n-i} + P_i$ )	40
Ring opening of aromatics ( $A_n \rightarrow P_n$ )	45
Hydrogenation of naphthenes ( $A_n \rightarrow N_n$ )	30

**Table 3** Exponential values of pressure (adapted from Elizalde and Ancheyta [7])

Reaction	$w$
Dehydrocyclization of paraffins	-0.700
Hydrocracking of paraffins	0.433
Dehydrogenation/hydrogenation of aromatics	0.000
Hydrodealkylation of aromatic and naphthenes	0.500
Other reactions	0.000

## Mathematical model

Modeling the behaviour of the reactions is done by solving the model equations describing the system. The equations describing the mass balance and heat balance are solved simultaneously on gPROMS as represented in Eqs. (52–57):

$$-\frac{dF}{dW} + \sum_{j=1}^{Nr} (r_j \gamma_j) = \frac{\epsilon d(ci)}{\rho b dt}, \quad (52)$$

$$\frac{dT}{dt} = \frac{-\left(\sum_{i=1}^{NC} F_i C P_i\right) + \frac{dT}{dW} \sum_{j=1}^{Nr} (r_j \gamma_j)(-\Delta H_{Rj})}{C_{p_{cat}} + \frac{\epsilon}{\rho b} \sum_{i=1}^{NC} C_i C P_i}, \quad (53)$$

$$\frac{dP}{dW} = \left[ 1.75 \times 10^{-5} \frac{(1-\epsilon)}{\epsilon^3} \frac{G^2}{\rho d_p g_C} + 1.5 \times 10^{-5} \frac{(1-\epsilon)}{\epsilon^3} \frac{G\mu}{\rho d_p^2 g_C} \right] \times \rho A, \quad (54)$$

$$\Delta H_R = \sum v_p H_{fp} - \sum v_r H_{fr}, \quad (55)$$

$$H_{ri} = H_{ri}^0 + \int_{298K}^T C_p dT, \quad (56)$$

$$C_p = A1 + B1T + C1T^2 + D1T^3. \quad (57)$$

Equations (26–50) are the rate equations for all the components, while Eq. (51) is the kinetic rate constant applied to all the rate equations.

Equation (52) is the material balance equation where  $\rho b$  is the bulk density and  $\epsilon$  the bed voidage. Equation (53) is the heat balance of the reaction to determine the temperature behaviour where  $-\Delta H_{Rj}$  is the heat of the reaction of the  $j$ th component and  $C_{p_{cat}}$  is the heat capacity of the catalyst. Equation (54) gives the pressure profile of the reaction where  $D_p$  is particle diameter,  $G$  the mass flux,  $\epsilon$  the bed voidage,  $\rho$  the gas density, and  $A$  the reactor area.  $H_{ri}^0$ , the standard heat of formation of the components and the constants of  $A1$ ,  $B1$ ,  $C1$ , and  $D1$  for the  $C_p$ , heat capacity, in Eqs. (56, 57), are taken from Riazi [18]. These equations are solved simultaneously using gPROMS to determine the behaviour of the system. gPROMS is a robust mathematical software that could solve all the four reactors in series dynamically given the behaviour of the paraffins, naphthenes and aromatics as well as the dynamics of the temperature in the reactors. All the components' behaviour was determined.

## RON model

The estimation of the RON of hydrocarbons for the feed and products can be done using different methods of prediction. RON can be calculated for each pure component using a polynomial equation that correlates to the normal boiling point [18] as shown by Eq. (58):

$$RON = Aa + BbT + CcT^2 + DdT^3 + EeT^4, \quad (58)$$

where  $T = TBP \times 0.01$ , TBP represents the normal boiling point ( $^{\circ}C$ ), and  $Aa$ ,  $Bb$ ,  $Cc$ ,  $Dd$ , and  $Ee$ , are coefficients. The RON of a hydrocarbon mixture is calculated by assuming that the mixture consists of paraffins, naphthenic hydrocarbons, and aromatics. The equation is expressed as the sum of the RON for each pure component multiplied by the volume fractions of the components.

## Model validation

The model validation was carried out by modeling and simulating the commercial data of Ancheyta et al. [2] and Rodríguez and Ancheyta [19] on gPROMS to ascertain the capability and ruggedness of the mathematical software in complex modeling. The modeling of Ancheyta et al. [2] was performed using MATLAB software and the result is compared with that obtained with gPROMS. The configuration of the commercial reformer and feed properties are given in Tables 4 and 5, respectively.



**Table 4** Configuration of commercial catalytic reformer [2]

Reactor number	Height (m)	Diameter (m)	Catalyst (kg)	WHSV ( $\text{h}^{-1}$ )
1	4.902	2.438	9130	16
2	5.410	2.819	13,820	10.6
3	6.452	2.971	22,820	6.4
4	8.208	3.505	42,580	3.4

**Table 5** Feed stock properties of commercial catalytic reformer [2]

Property	
MW (g/gmol)	104.8
Specific gravity	0.7406
IBP ( $^{\circ}\text{C}$ )	88
10%	101
90%	155
EBP ( $^{\circ}\text{C}$ )	180
Total paraffins (mol%)	59.11
Total naphthenes (mol%)	20.01
Total aromatics (mol%)	20.88

## Model validation results

The commercial reformer Ancheyta et al. [2] were simulated with the properties of Tables 4 and 5, respectively,

with four semi regenerative reactors in series. The reformer's throughput is 30 MBPD at inlet temperature of 495  $^{\circ}\text{C}$  and pressure of 10.5  $\text{kg}/\text{cm}^2$  using MATLAB mathematical tool on ODE45. The simulation was performed on gPROMS software to validate its capability in modeling this problem. The result obtained from gPROMS is compared with that obtained with MATLAB from Ancheyta et al. [2], and presented in Table 6.

From the modeling and simulation results, the Ancheyta et al.'s [2] result and that of gPROMS were compared and analyzed. The result showed a good and comparable result between the actual and that simulated with gPROMS. This is an indication of the capability of the mathematical tool in solving complex model equations

## Results and discussion

### Simulation analysis

The model was validated with commercial data from Ancheyta et al. [2] and Rodríguez and Ancheyta [19] and Kaduna refinery and petrochemical company (KRPC), and shows good agreement with data from both sources. The commercial plant modeling and simulation results are in good agreement, as shown in Fig. 3 and Table 7. Tables 8

**Table 6** Comparison between results from MATLAB [2] and gPROMS

Components	Actual (mol%)	Simulated Ancheyta et al. [2] (mol%)	Simulated gPROMS (mol%)	Absolute difference Ancheyta et al. [2] (mol%)	Absolute difference gPROMS (mol%)
$P_5$	4.83	5.37	5.94	0.21	1.11
$P_6$	15.08	15.17	13.18	0.25	1.9
$P_7$	11.2	11.32	11.31	0.28	0.11
$P_8$	4.79	4.44	5.52	0.18	0.73
$P_9$	2.3	2.20	2.21	0.10	0.09
$P_{10}$	0.15	0.16	0.33	0.01	0.18
$P_{11}$	0.01	0.01	0.00	0.00	0.01
MCP	1.25	1.22	1.23	0.11	0.02
$N_6$	0.19	0.07	0.23	0.04	0.04
$N_7$	0.38	0.35	0.50	0.03	0.12
$N_8$	0.59	0.56	0.36	0.03	0.23
$N_9$	0.14	0.15	0.11	0.01	0.03
$N_{10}$	0.02	0.02	0.023	0.00	0.003
$N_{11}$	0.00	0.00	0.00	0.00	0
$A_6$	5.43	5.68	5.36	0.25	0.07
$A_7$	15.03	14.96	13.62	0.07	0.41
$A_8$	18.63	19.22	17.78	0.61	0.85
$A_9$	13.68	13.07	12.15	0.61	1.53
$A_{10}$	4.72	4.56	4.34	0.16	0.38
$A_{11}$	1.58	1.51	1.32	0.07	0.26

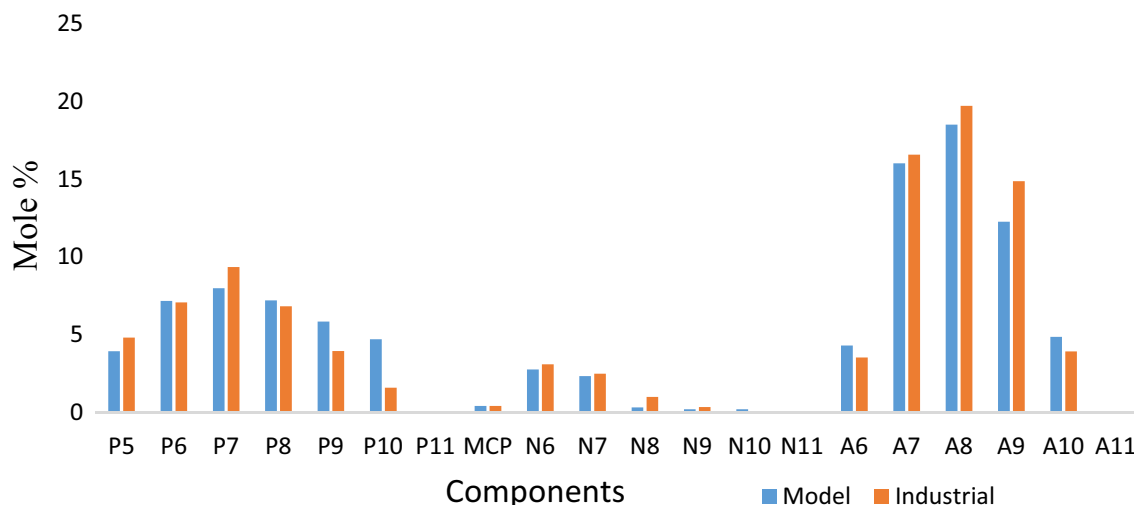


**Fig. 3** Comparison between model simulation and industrial plant data

and 9 show the configuration and feed properties of KRPC commercial catalytic reformer.

Figure 4 shows the concentration profile of paraffins along the reactor height.  $P_5$ ,  $P_6$ ,  $P_7$ ,  $P_8$ ,  $P_9$ , and  $P_{10}$  are paraffins with hydrocarbon numbers 5, 6, 7, 8, 9, and 10, respectively. Normal paraffin components basically undergo three major reactions during naphtha reforming. Firstly, they undergo hydrocracking to lighter paraffins, i.e., methane, ethane, propane, and butane, as shown in reactions 8–33 in Table 1. Secondly, the isomerization reaction to form isoparaffins. This is a slow reaction with slow reaction rate, hence, it is not considered in this work. Thirdly, the dehydrocyclization to naphthenes, a very slow reaction, leads to a decrease in the paraffins. These reactions are reactions 1–7 from Table 1. Dehydrocyclization reaction becomes easier as the molecular weight of the paraffins increases as in  $P_8$ ,  $P_9$ , and  $P_{10}$ , while  $P_7$  shows little increase.  $P_5$  and  $P_6$  increase due to hydrocracking. The main effects of hydrocracking are decrease of paraffins ( $C_5^+$ ) in the reformat, decrease in hydrogen production, and increase in LPG production and hydrogenolysis. The isomerization reactions are fast, slightly exothermic and do not affect the number of carbon atoms. The thermodynamic equilibrium of isoparaffins to paraffins depends mainly on the temperature and pressure which has no effect. The paraffins isomerization results in a slight increase of the octane number. These reactions are promoted by the acidic function of the catalyst support. The paraffin dehydrocyclization step becomes easier as the molecular weight of the paraffin increases. From Table 1, the rates increase from 0.00, 0.58, 1.33, 1.81, and 2.54 for  $P_6$ – $P_{11}$ . However, the tendency of paraffins to hydrocrack increases concurrently. Kinetically, the rate of dehydrocyclization increases with low pressure and high temperature. To sum up, the dehydrocyclization of  $P_6$  paraffins to benzene is

**Table 7** Relative errors between industrial and simulated results of KRPC plant

Component	Simulated (mol%)	Industrial (mol%)	Absolute error
$P_5$	4.22	4.81	0.595
$P_6$	7.16	7.07	0.089
$P_7$	8.22	9.35	1.135
$P_8$	7.20	7.01	0.194
$P_9$	5.84	3.94	1.902
$P_{10}$	4.70	1.59	3.111
MCP	0.42	0.42	0
$N_6$	2.76	3.09	0.326
$N_7$	2.34	2.49	0.152
$N_8$	0.31	0.68	0.365
$N_9$	0.20	0.34	0.136
$N_{10}$	0.19	0.12	0.077
$A_6$	4.29	3.53	0.764
$A_7$	16.02	16.57	0.550
$A_8$	18.71	19.72	1.009
$A_9$	12.27	14.87	2.597
$A_{10}$	4.86	4.21	0.646

**Table 8** Configuration of KRPC commercial catalytic reformer (Chi-yoda, 1980 #293)

Reactor number	Height (m)	Diameter (m)	Catalyst (kg)	WHSV ( $h^{-1}$ )
1	5.63	1.9	9572	5.56
2	5.83	2.1	12,119	4.39
3	6.51	2.3	16,231	3.28
4	7.26	2.7	24,938	2.13

**Table 9** Feed properties of KRPC commercial catalytic reformer

	Feed stock properties
MW (g/gmol)	103.7
SG	0.76
IBP (°C)	88
5%	97
10%	102
15%	110
30%	118
50%	131
75%	147
95%	152
EBP (°C)	170
RVP (bar)	0.97
Sulfur (ppm)	0.32

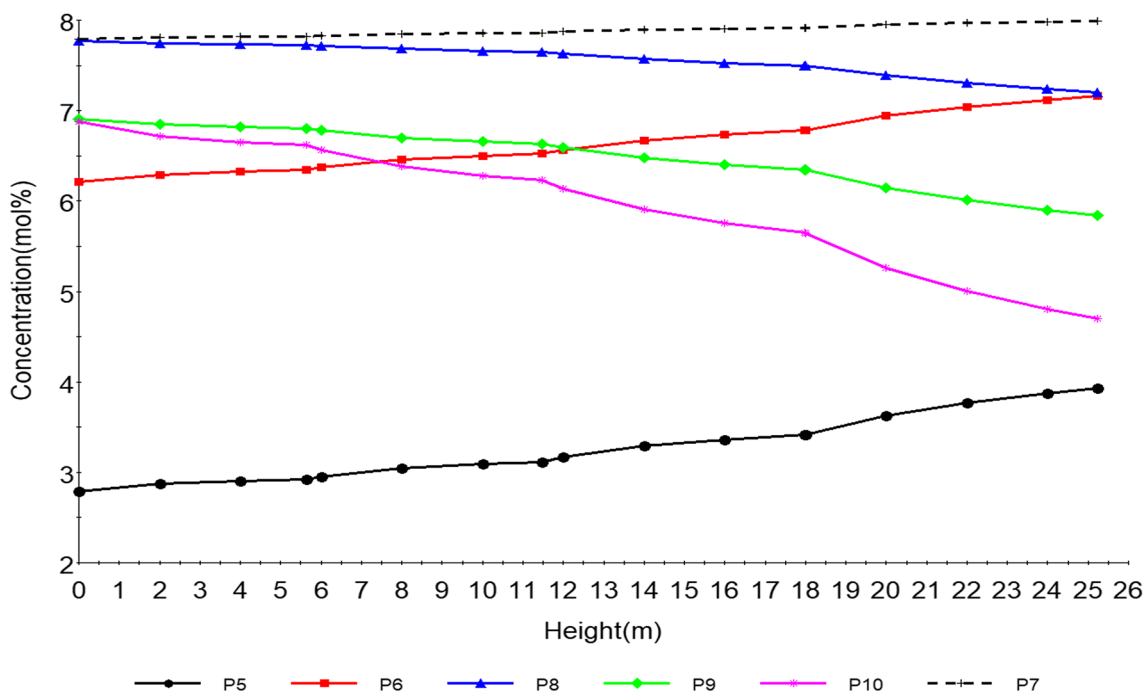
more difficult than that of C<sub>7</sub> paraffin to toluene, which itself is more difficult than that of C<sub>8</sub> paraffin to xylenes. Accordingly, the most suitable fraction to feed a reforming process is the C<sub>7</sub>–C<sub>10</sub> fraction.

Figure 5 shows the behaviour of the naphthenes along the reactor height. N<sub>6</sub>, N<sub>7</sub>, N<sub>8</sub>, N<sub>9</sub>, and N<sub>10</sub> are naphthenes with hydrocarbon number 6, 7, 8, 9, and 10, respectively. The fastest reaction is aromatization, i.e., dehydrogenation of naphthenes, resulting in the large temperature drop due to its highly endothermic nature. The drastic reduction is due to the aromatization to aromatics. Thermodynamically, the

reaction is highly endothermic and is favored by high temperature and low pressure. In addition, the higher the number of carbon atoms, the higher the aromatics production at equilibrium from N<sub>8</sub>, N<sub>9</sub>, and N<sub>10</sub>. This can be seen from Table 1 in Eqs. (34–39) where the reaction rates increase from 4.02, 9.03, 21.5, 24.5, and 24.5, respectively, for N<sub>6</sub>, N<sub>7</sub>, N<sub>8</sub>, N<sub>9</sub>, and N<sub>10</sub>. From a kinetic point of view, the rate of reaction increases with temperature. The naphthenes also undergo hydrocracking to lighter hydrocarbons leading to their decrease as shown in reactions (49–57) in Table 1.

Figure 6 shows the behaviour of aromatics along the reactor height. A<sub>6</sub>, A<sub>7</sub>, A<sub>8</sub>, A<sub>9</sub>, and A<sub>10</sub> are paraffins with hydrocarbon numbers 5, 6, 7, 8, 9, and 10, respectively. The dehydrogenation of naphthenes, as shown in Fig. 5, increases the aromatics, as shown in Fig. 6. The sharp increase is because of drastic aromatization of the naphthenes favored by the metallic sites of the catalyst. The rate of benzene formation is lower due to lower carbon number of N<sub>6</sub>, while A<sub>7</sub>, A<sub>8</sub>, and A<sub>9</sub> increase rapidly due to higher carbon number of N<sub>7</sub>, N<sub>8</sub>, and N<sub>9</sub>.

Figure 7 shows the temperature profile of the reactions along the reactor height and the sharp drop in first and second reactors is due to the more endothermic dehydrogenation reaction of naphthenes to aromatics. Typically, dehydrogenation and isomerization reactions take place in the first reactor, dehydrogenation, isomerization, dehydrogenation, and cracking in the second followed by dehydrogenation and cracking in the third and fourth reactors.



**Fig. 4** Concentration profile of paraffins with changing reactor height

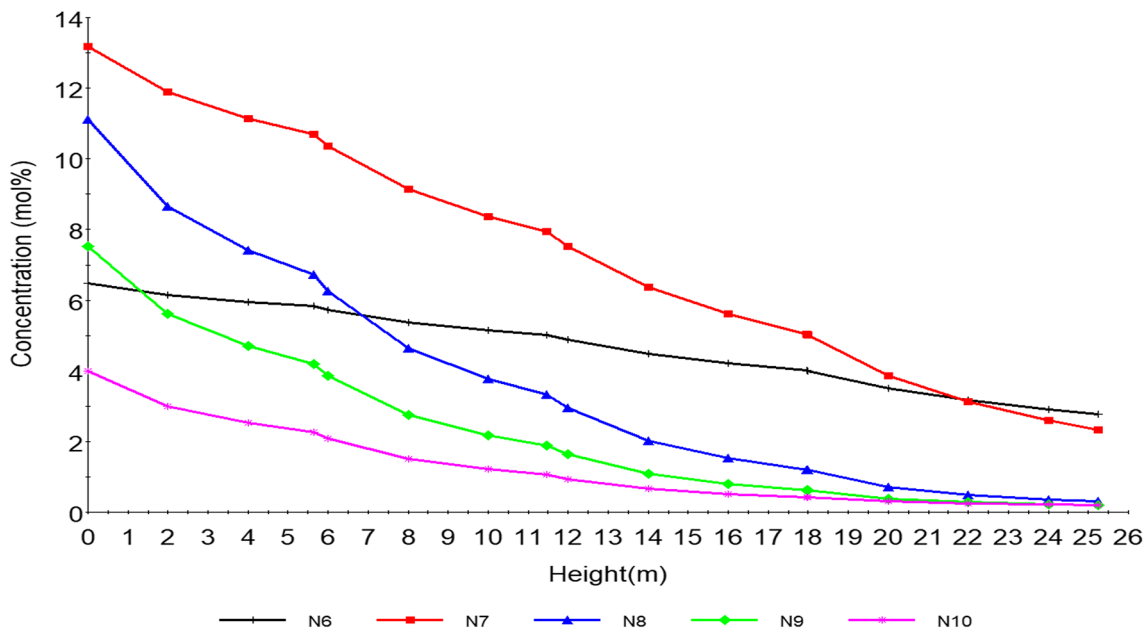


Fig. 5 Concentration profile of naphthenes with changing reactor height

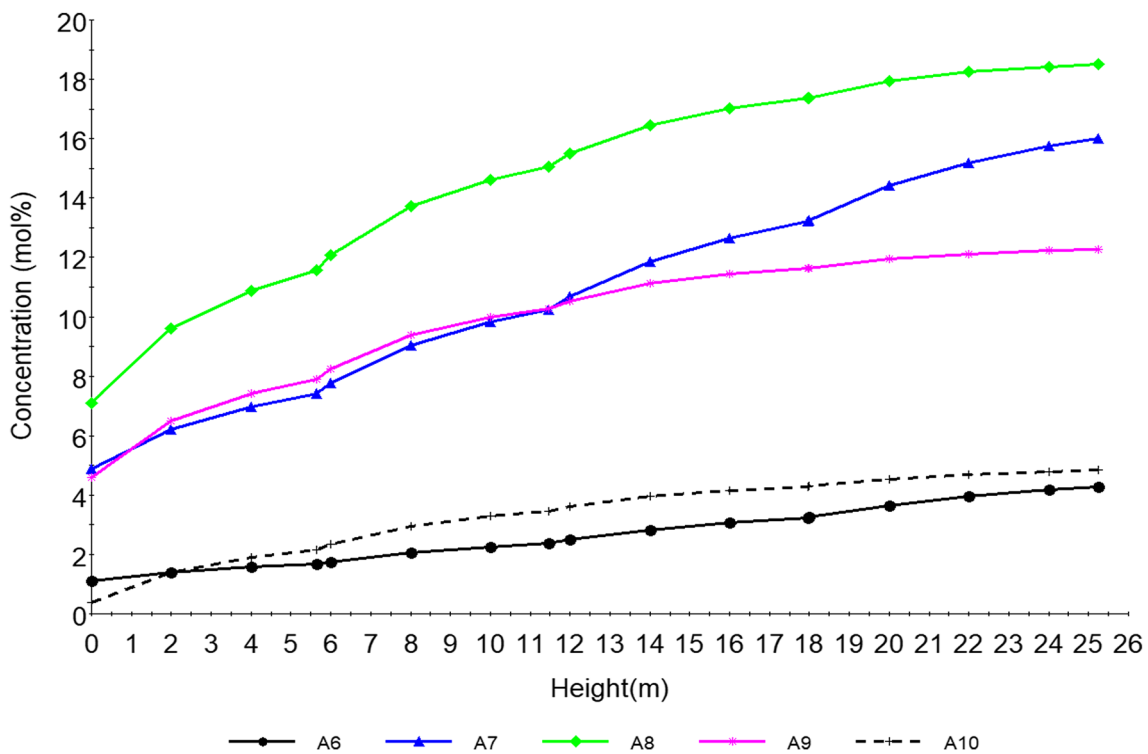


Fig. 6 Concentration profile of aromatics with changing reactor height

Figures 8 and 9 show how the increase in hydrogen yield and RON varies, respectively, along the height of the reactor. This is due to the increase in the aromatics along the reactor

height. The RON increases from reactor one to four due to increase in aromatization reaction, which gives a higher research octane number, a parameter for antiknock in the

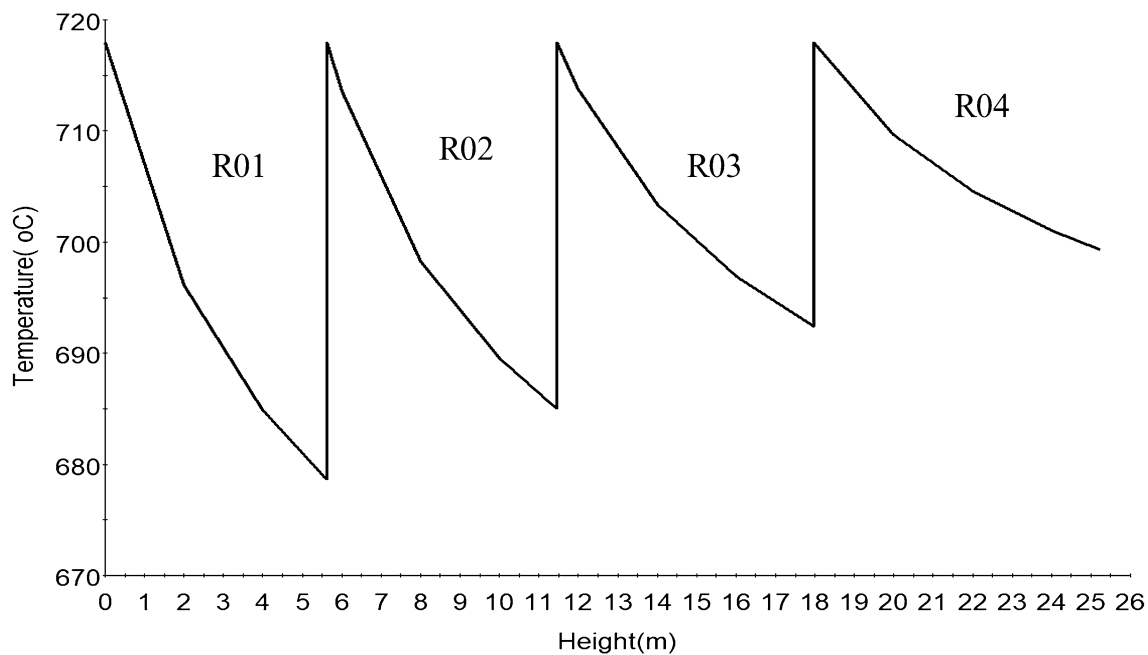


Fig. 7 Temperature profile with changing reactor height

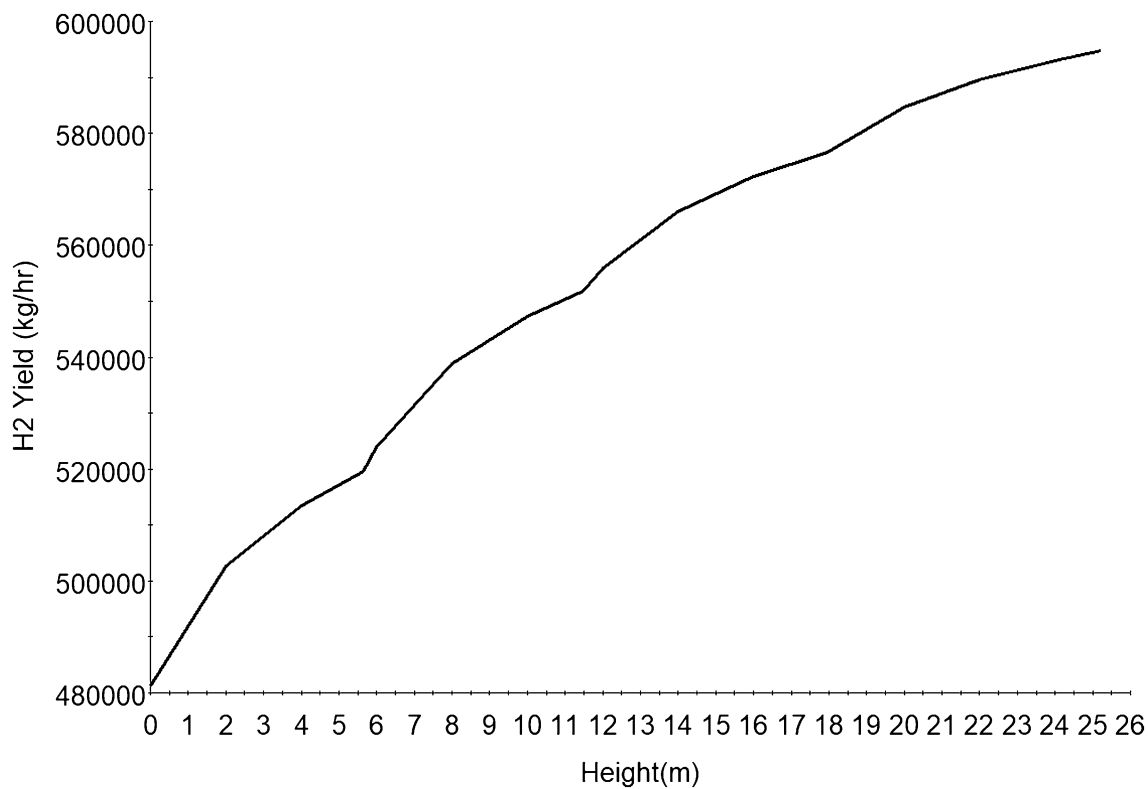
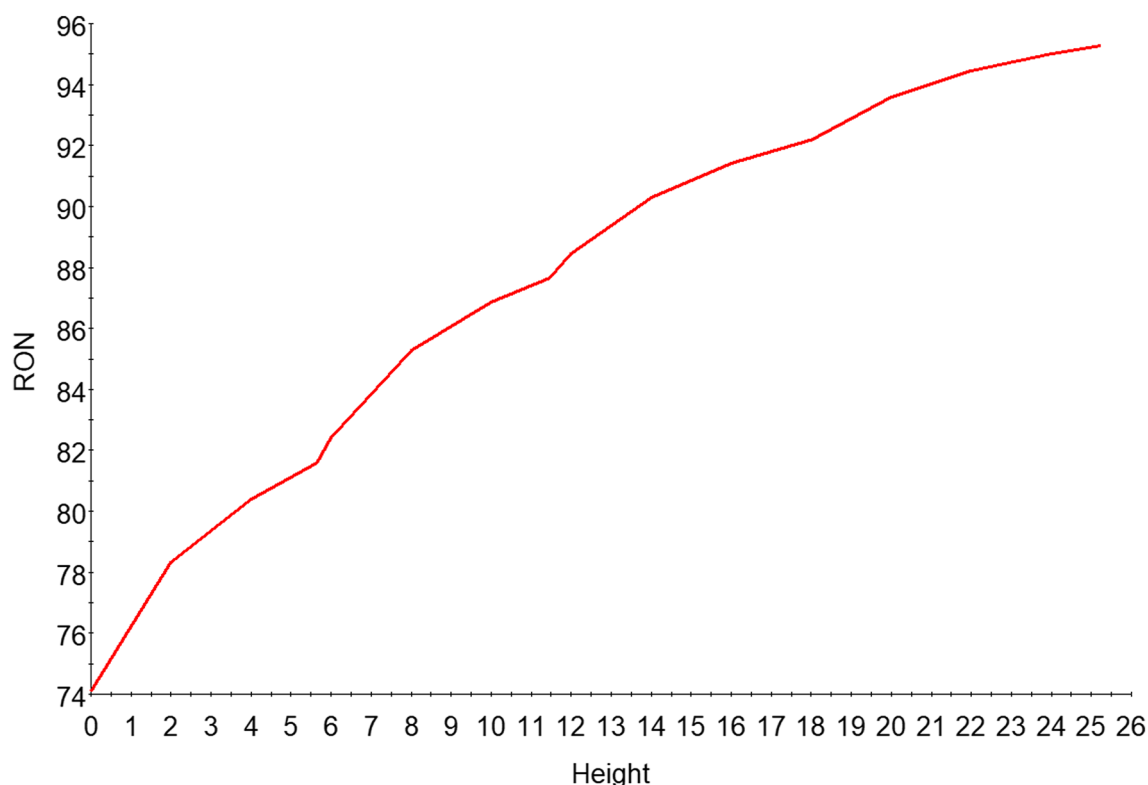


Fig. 8 H<sub>2</sub> yield along the four reactors height



**Fig. 9** RON along the reactor height

gasoline engine. Treated naphtha has low RON and cannot be used as gasoline, hence the reforming reaction of the components to give a gasoline with higher research octane number.

### Analysis of compressibility factor

In this study, initially, the compressibility factors of different empirical correlations were added to catalytic-reforming reactor model using HHR of 6.4. The pressure profile of the four reactors in series is given in Fig. 10. The pressure decreases continually from the first reactor and decreases from 18.65 to 12.6 kPa at the exit of the last reactor. In Fig. 11, the profile of the gas densities behaves in similar way due to the drop and decrease in the reactors pressure, but the last reactor exhibits a slightly different behaviour due to the larger pressure drop in the last reactor.

Figure 12 shows the compressibility factor profiles along the reactor heights of the different correlations used. The correlation of Shokir et al. [21] gave a non-zero  $Z$  factor along the reactor heights, because the range of  $P_{pr}$  and  $T_{pr}$  is wider than others. The Heidaryan et al.'s [12] compressibility factor was negative and thus would not give meaningful data and so it is not reported. The  $Z$  factor changes along the reactor heights due to the variation of operational conditions and transport properties aforementioned. The  $Z$

factor at each height of reactor is not the same, and it is obvious that if these variables change with the  $Z$  factors as in Fig. 12, the  $Z$  factor cannot be a constant value of unity as always assumed. The Mahmoud [16]  $Z$  factor is the closest to the ideal compared to others, although this does not signify that it is the true representation of the  $Z$  factors, but further analysis will be carried out on how it correlates or deviates from other process variables in the reactors. Factors such as the yield of reformat, hydrogen, and aromatics yield for each compressibility correlation, and the temperature and pressure profiles along the reactors' heights will need to be considered as well.

ZB represents Bahadori et al. [4], ZH1 represents Heidaryan et al. [11], ZM represents Mahmoud [16], ZP represents Papay [17], ZS represents Sanjari and Lay [20], and ZSH represents Shokir et al. [21].

Figure 13 shows the profiles of the density of the gas phase along the reactor heights. Gas density is a function of pressure and temperature as well as feed flow rate. The pressure model equation is also a function of gas density as in Eq. (54). Therefore, the density is significant in determining the  $Z$  compressibility factors and the pressure profiles. The density profile decreases along the reactor height due to the drop in temperature across the various reactors. The behaviour is true for all the correlations and Fig. 12 shows that the  $Z$  factors have different profiles of gas densities. However,



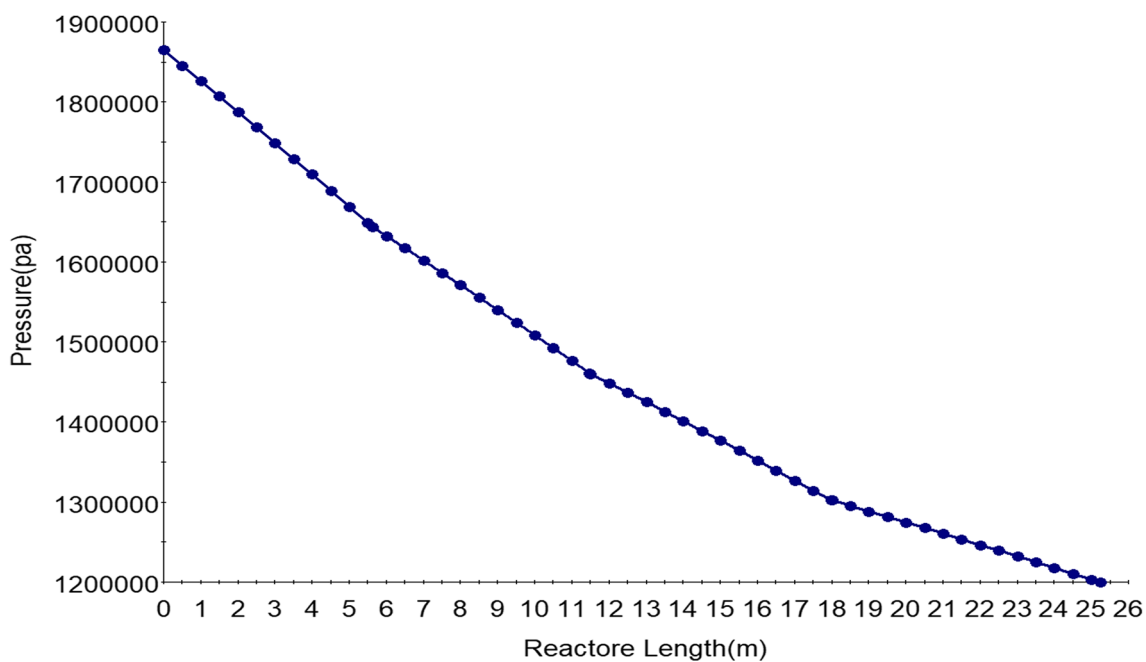


Fig. 10 Pressure profile with changing reactor height



Fig. 11 Gas density profile with changing reactor height

in Fig. 13, the profile of gas density for Papay [17] is the closest to that of the density for ideal vapor unlike Fig. 12 where the compressibility factor correlation of Mahmoud [16] is the closest. This implies that further analysis needs to be carried out.

The temperature variation with Z factor, as shown in Fig. 14, has effect on the product quality and yield generally

as a result of the effect of the kinetic equations which are dependent on reaction temperature. Therefore, enthalpy of various compressibility factors correlations could also vary simultaneously, but the effect is obvious in the last reactor temperature decrease, as shown in Fig. 14. Figure 15 shows reformat yield along the reactors' heights of various Z factor correlations. As with the case of temperature,

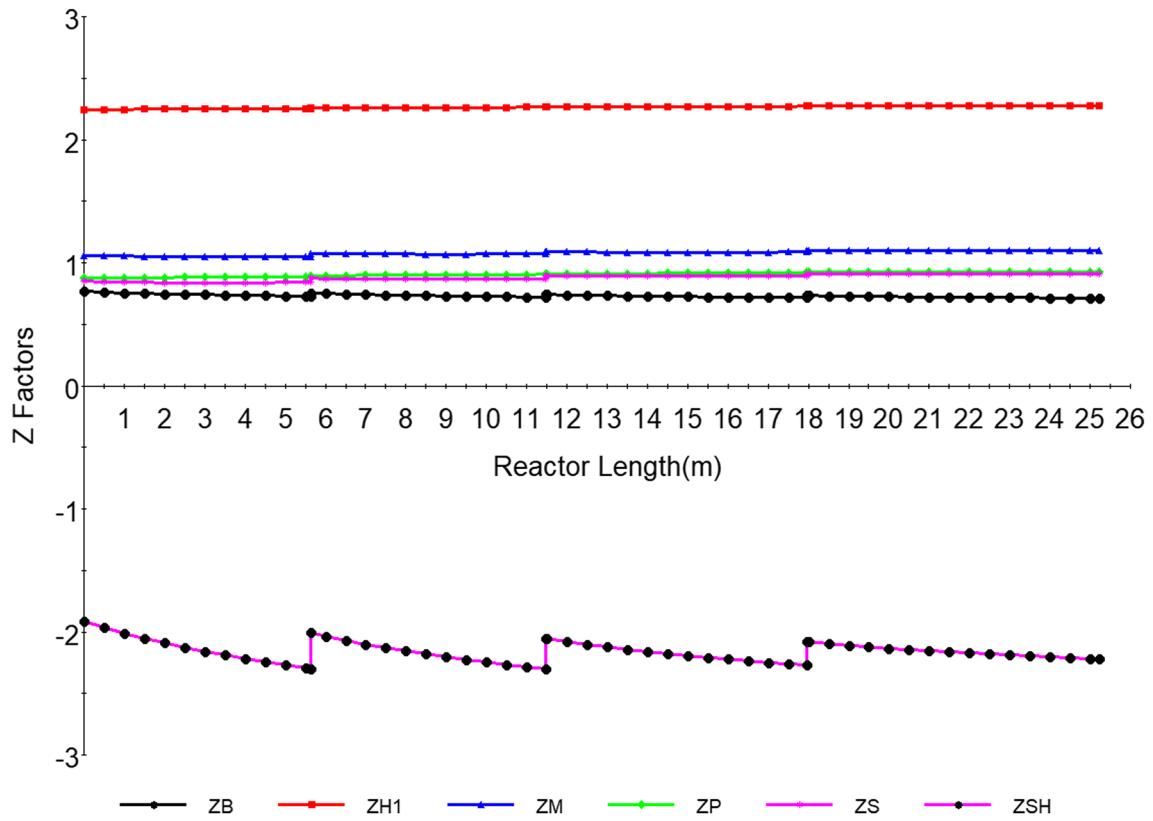


Fig. 12 Compressibility Z factor profiles

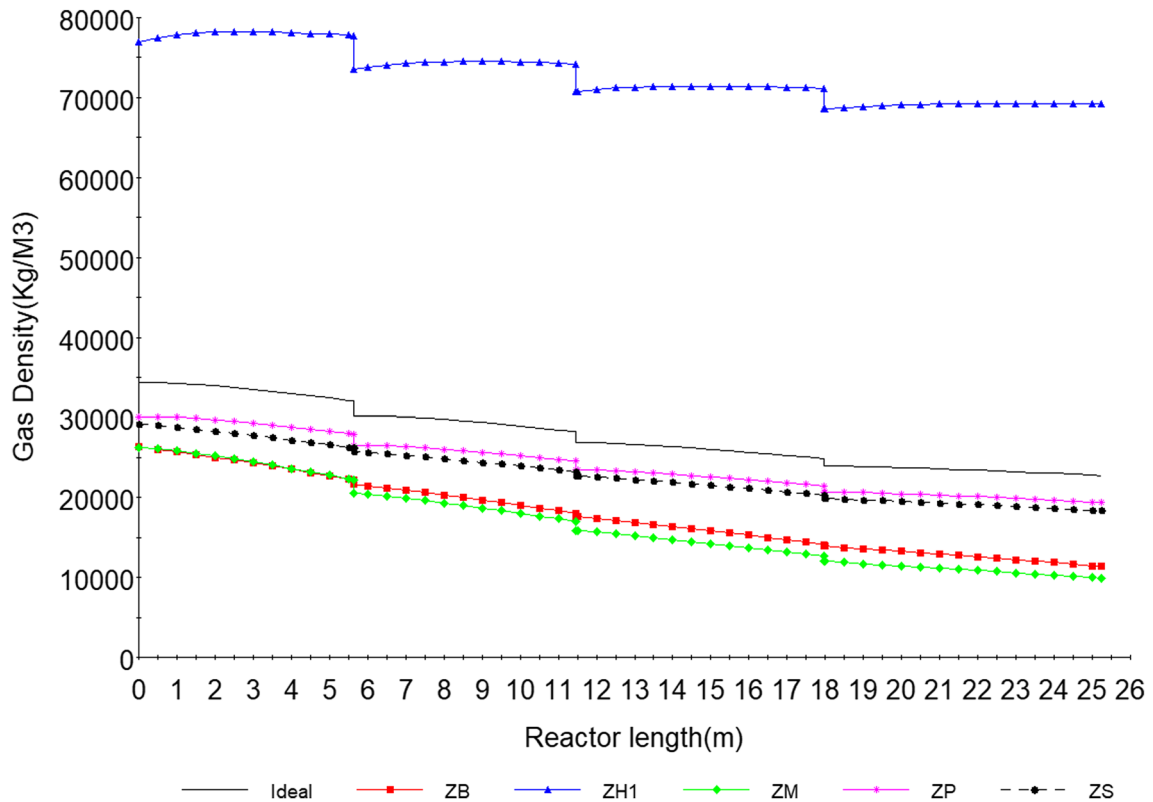


Fig. 13 Density profile along the reactors

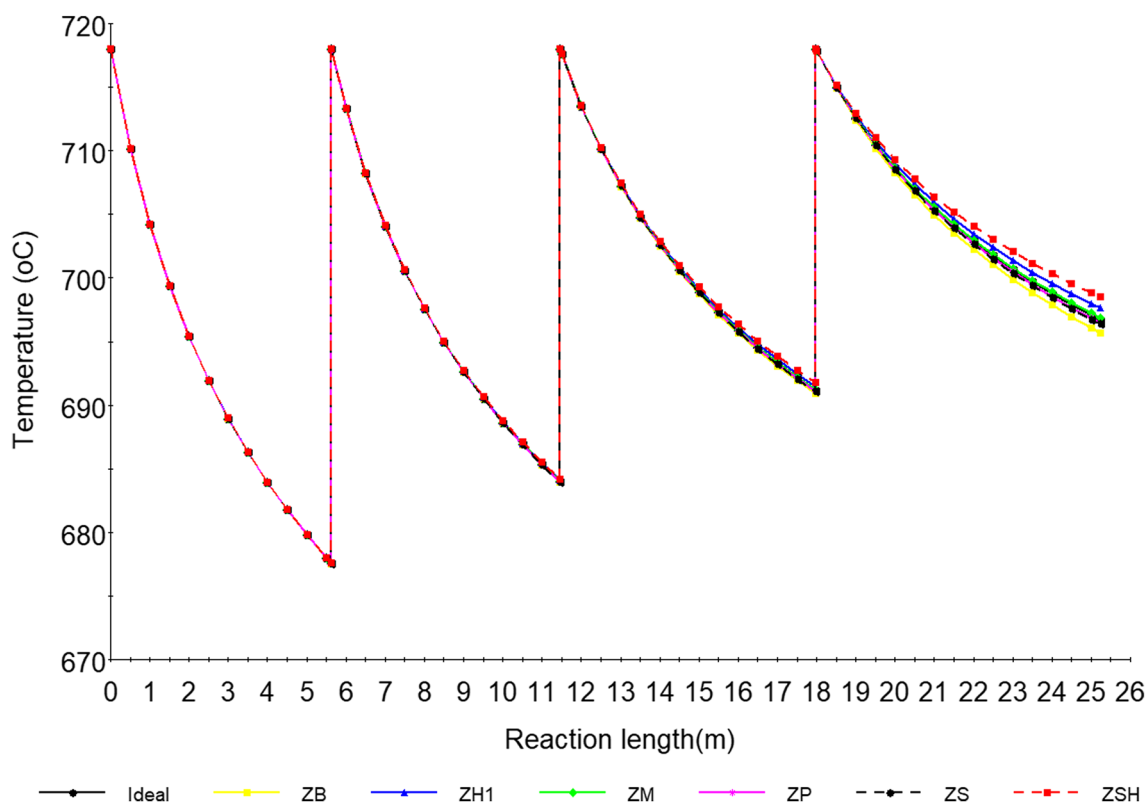


Fig. 14 Temperature profile along the reactors

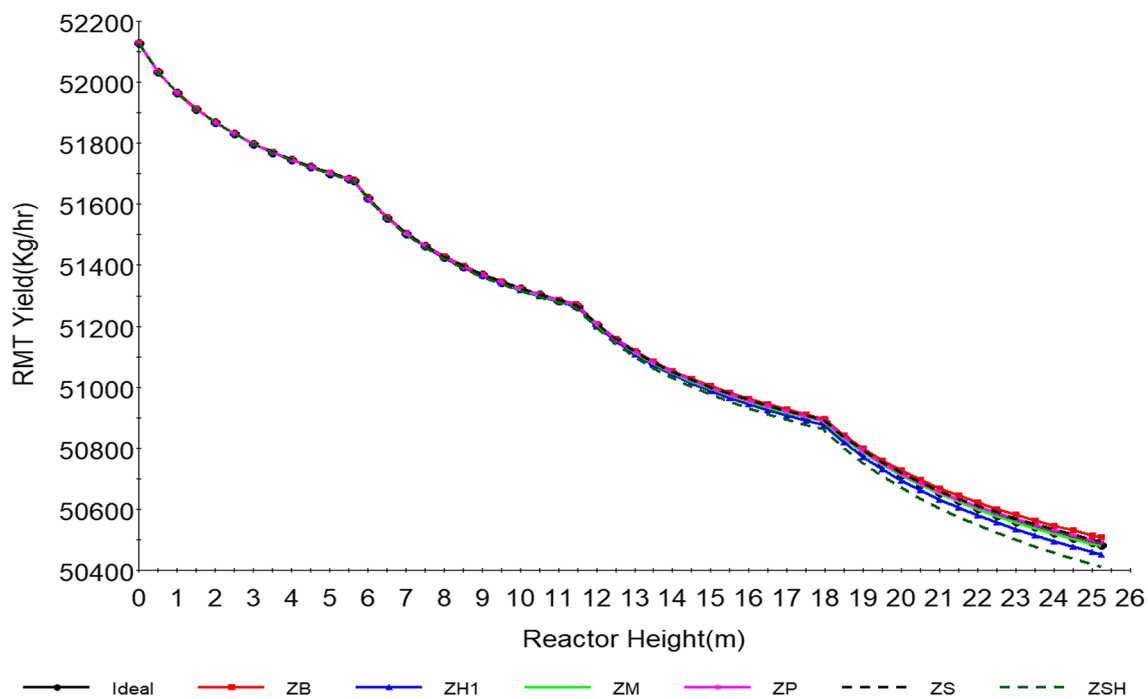


Fig. 15 RMT profile along the reactors

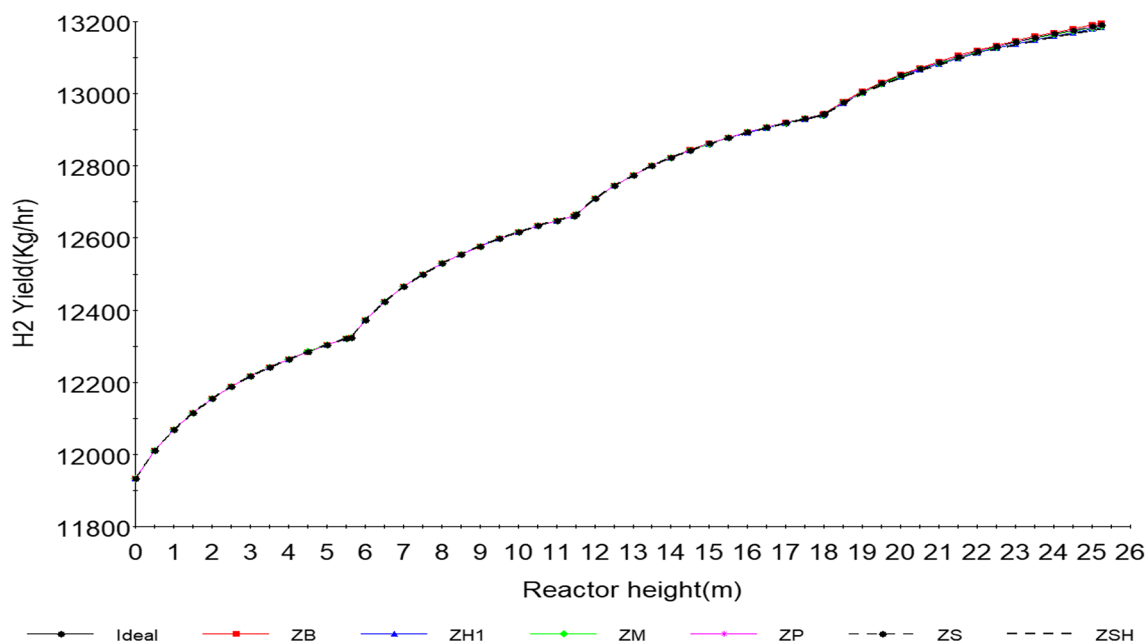


Fig. 16 Hydrogen profile along the reactors

**Table 10** RMT and hydrogen yields at the outlet of the fourth reactor

Z factor	RMT yield (kg/h)	% difference	H <sub>2</sub> yield (kg/h)	% difference
Ideal	50,483.297	0.00	13,187.961	0.00
ZB [4]	50,508.75	0.049	13,194.625	0.050505
ZH1 [11]	50,451.57	-0.0629	13,183.403	-0.03457
ZM [16]	50,479.39	-0.0077	13,187.231	-0.00554
ZP [17]	50,491.18	0.016	13,189.628	0.012639
ZS [20]	50,494.31	0.02	13,190.367	0.018241
ZSH [21]	50,411.51	-0.142	13,180.737	-0.05481

**Table 11** Pressure drop (Pa) across the four reactors for various Z factor correlations at HHR 6.0

Z factor	R01 outlet	R02 outlet	R03 outlet	R04 outlet
Ideal	1,655,242.0	1,484,220.0	1,336,286.8	1,241,587.1
ZB [4]	1,576,799.1	1,325,251.8	1,087,961.0	919,812.3
ZH1 [11]	1,774,789.5	1,706,555.8	1,651,777.4	1,618,936.6
ZM [16]	1,666,173.2	1,508,018.4	1,374,495.0	1,290,825.0
ZP [17]	1,625,020.0	1,429,442.4	1,259,440.1	1,149,702.5
ZS [20]	1,612,015.6	1,406,727.8	1,228,460.8	1,113,143.4
ZSH [21]	1,955,957.6	2,018,512.0	2,065,850.1	2,093,332.2

where the enthalpy of reactions has a pronounced effect, the pressure, HHR, the reformat yield, and hydrogen yield also change due to the variation of the different Z factors as shown in Figs. 15 and 16. For the reformat and hydrogen

yields, Table 10 gives the different exit values of the RMT and hydrogen yields with the values from the Mahmoud [16] being the closest.

For an accurate prediction of a suitable compressibility factor correlation for the CRU modeling, a study of the hydrogen-to-hydrocarbon ratio, which is a major dynamic variable that influences the reaction hydrodynamics, is performed. The variation of reaction pressure is investigated also for the compressibility empirical correlations and a comparison with the pressure values of the model results and that of the ideal case is depicted in Fig. 15

The various pressures vary along the reactor height with some above the ideal gas correlations and some below are shown in Fig. 17. The closest to ideal behaviour is the Mahmoud Z factor correlation [16].

Since the Mahmoud's [16] compressibility factor correlation is the closest to that of the ideal case, a further analysis is performed between the two by varying the pressure of the reaction and the HHR. This will give the extent of closeness of the product distribution. Tables 7 and 8 show the pressure drops with variation in HHR, while Fig. 16 shows the effects of variation of the pressure using the Mahmoud correlation with Z equal to one. For HHR of 6.4, it has a 0.709% deviation at the exit of the first reactor, 1.734% at the exit of the second reactor, 3.118% at the exit of the third reactor, and 4.343% at the exit of the fourth reactor.

For HHR of 7.0, it has a 0.796% deviation at the exit of the first reactor, 2.00% at the exit of the second reactor, 3.720% at the exit of the third reactor, and 5.319% at the exit of the fourth reactor. The decrease in pressure for the various

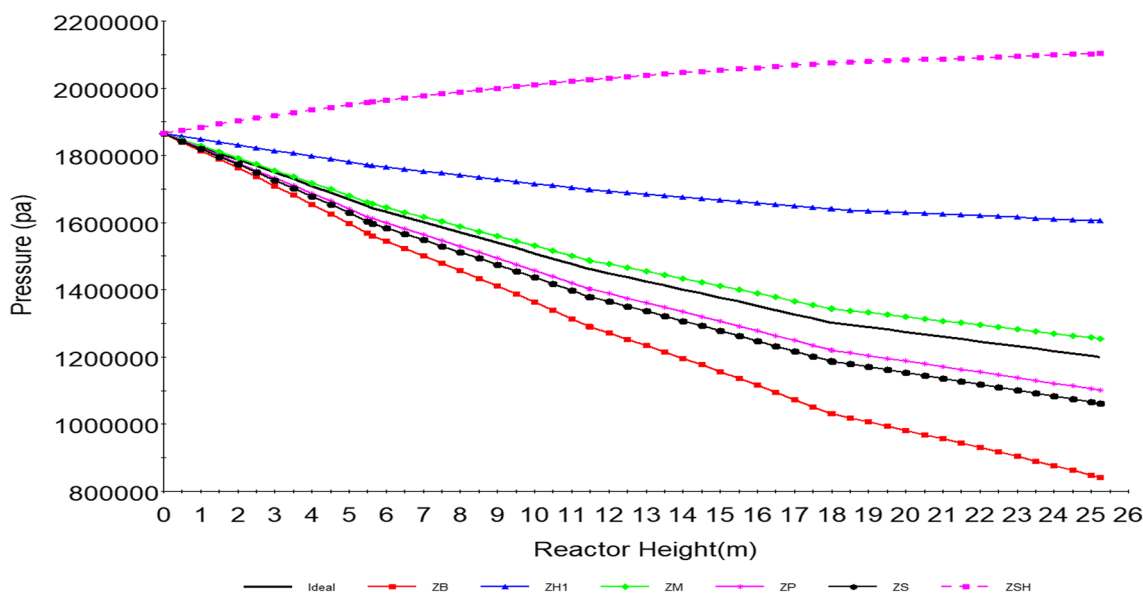


**Fig. 17** Pressure profile along the reactors for different compressibility correlations. The decrease in pressure for the various empirical correlations for different HHR ratios is given in Table 11. The closest among them to the ideal is Mahmoud [16]. It has 0.65% deviation at

the exit of the first reactor, 1.58% at the exit of the second reactor, 2.78% at the exit of the third reactor, and 3.814% at the exit of the fourth reactor

**Table 12** Pressure drop (Pa) across the four reactors for various Z factor correlations at HHR 6.4

Z factor	R01 outlet	R02 outlet	R03 outlet	R04 outlet
Ideal	1,643,579.0	1,461,651.9	1,302,852.5	1,200,254.8
ZM [16]	1,655,322.5	1,487,492.1	1,344,794.9	1,254,760.5
% difference	0.709	1.737	3.118	4.344

**Table 13** Pressure drop (Pa) across the four reactors for various Z factor correlations at HHR 7.0

Z factor	R01 outlet	R02 outlet	R03 outlet	R04 outlet
Ideal	1,625,363.6	1,426,021.9	1,249,352.6	1,133,334.1
ZM [16]	1,638,408.6	1,455,221.9	1,297,629.1	1,197,010.5
% difference	0.796	2.0065	3.720	5.319

empirical correlations for different HHR ratios of 6.4 and 7.0 is given in Tables 12 and 13.

The increase in pressure shows a match between the Mahmoud’s [16] correlation and the ideal, as shown in Fig. 18. At the different exit of the reactor, the temperatures are different due to fall in temperature. The Z compressibility factors are different which are functions of the gas densities which are functions of pressure. The Mahmoud [16] correlation becomes more suitable and applicable at a higher pressure and lower HHR.

### Conclusion

A detailed steady-state model of catalytic-reforming unit (CRU) of four reactors in series is modeled in this work and a simulation with various compressibility factors is performed using gPROMS, a mathematical and modeling software. The conclusions are:

1. The simulated results from this study are compared with data from the KRPC industrial plant. The parameters of both kinetic and thermodynamic are obtained from the open literature [7]. Good agreement between the simulated and plant data shows the robust strength and capability of the gPROMS model builder in modeling and simulating four reactors in series. Therefore, gPROMS

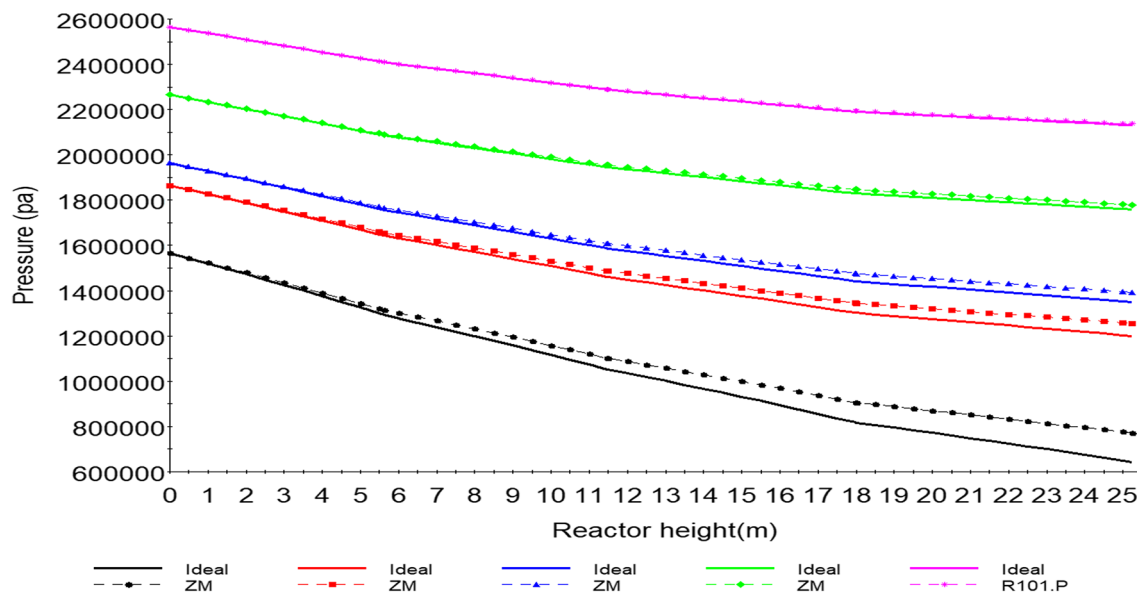


**Fig. 18** Effects of variation of the pressure with Mahmoud's [16] correlation with ideal at different height

can be recommended for modeling complex processes such as simulation of the CRU unit.

- Mahmoud's [16] compressibility  $Z$  factor is found to be a more suitable correlation in predicting the  $Z$  factor across the four reactors.
- Different yields of profiles for process variables such as density, reaction pressure, and enthalpy of reaction are obtained with corresponding different compressibility factors in the simulation of the CRU using the same process conditions. These profiles are as a result of varying temperature profiles and varying RMT yield as well as hydrogen yield.
- The pressure in each reactor is not the same for different HHR ratios. The reaction pressure is also not the same in each of the reactors when the Mahmoud [16] compressibility  $Z$  factor correlation is applied rather than assuming and treating the vapor as an ideal gas.

- The pressure drops across the four reactors are similar and comparable when Mahmoud's [16] correlation is applied and gives almost the same result at an inlet pressure of 2265 kPa. Hence, Mahmoud's [16] correlation can be used in modeling the pressures in CRU.

**Open Access** This article is distributed under the terms of the Creative Commons Attribution 4.0 International License (<http://creativecommons.org/licenses/by/4.0/>), which permits unrestricted use, distribution, and reproduction in any medium, provided you give appropriate credit to the original author(s) and the source, provide a link to the Creative Commons license, and indicate if changes were made.

## Appendix A

Tables 14, 15, 16, 17 and 18 are parameters adopted from the literature

**Table 14** Tuned coefficients for  $Z$  factor [3]

Coefficients	Fine-tuned coefficient	Coefficients	Fine-tuned coefficient
$a$	0.0373142485385592	$k$	-24,449,114,791.1531
$b$	-0.0140807151485369	$l$	19,357,955,749.3274
$c$	0.0163263245387186	$m$	-126,354,717,916.607
$d$	-0.0307776478819813	$n$	623,705,678.385784
$e$	13,843,575,480.943800	$o$	17,997,651,104.3330
$f$	-16,799,138,540.763700	$p$	151,211,393,445.064
$g$	1,624,178,942.6497600	$q$	139,474,437,997.172
$h$	13,702,270,281.086900	$r$	-24,233,012,984.0950
$i$	-41,645,509.896,474,600	$s$	18,938,047,327.5205
$j$	237,249,967,625.01300	$t$	-141,401,620,722.689



**Table 15** Tuned coefficients for Z factor [4]

Coefficients	Fine-tuned coefficients
<i>Aa</i>	0.969469
<i>Ba</i>	−1.349238
<i>Ca</i>	1.443959
<i>Da</i>	−0.36860
<i>Ab</i>	−0.107783
<i>Bb</i>	−0.127013
<i>Cb</i>	0.100828
<i>Db</i>	−0.012319
<i>Ac</i>	0.018481
<i>Bc</i>	0.052341
<i>Cc</i>	−0.050688
<i>Dc</i>	0.01087
<i>Ad</i>	−0.000584
<i>Bd</i>	−0.002146
<i>Cd</i>	0.002096
<i>Dd</i>	−0.000459

**Table 16** Tuned coefficients for  $0.2 \leq P_{pr} \leq 3$  [11]

Coefficients	Fine-tuned coefficient
$A_1$	2.827793
$A_2$	−0.4688191
$A_3$	−1.262288
$A_4$	−1.536524
$A_5$	−4.535045
$A_6$	0.06895104
$A_7$	0.1903869
$A_8$	0.6200089
$A_9$	1.838479
$A_{10}$	0.4052367
$A_{11}$	1.073574

**Table 17** Tuned coefficients for Z factor [12]

Coefficients	Fine-tuned coefficients
$A_1$	1.11532372699824
$A_2$	−0.07903952088760
$A_3$	0.01588138045027
$A_4$	0.00886134496010
$A_5$	−2.16190792611599
$A_6$	1.15753118672070
$A_7$	−0.05367780720737
$A_8$	0.01465569989618
$A_9$	−1.80997374923296
$A_{10}$	0.95486038773032

**Table 18** Tuned coefficients for Z factor [20]

Coefficients	Fine-tuned coefficient
$A_1$	0.007698
$A_2$	0.003839
$A_3$	−0.467212
$A_4$	1.018801
$A_5$	3.805723
$A_6$	−0.087361
$A_7$	7.138305
$A_8$	0.083440

## References

- Ahmed T (2001) Reservoir engineering handbook, 2nd edn. Elsevier, Amsterdam
- Ancheyta J, Villafuerte-Macias E, Diaz-Garcia L, Gonzalez-Arredondo E (2001) Modeling and simulation of four catalytic reactors in series for naphtha reforming. *Energy Fuels* 15(4):887–893
- Azizi N, Behbahani R, Isazadeh MA (2010) An efficient correlation for calculating compressibility factor of natural gases. *J Nat Gas Chem* 19(6):642–645
- Bahadori A, Mokhtab S, Towler BF (2007) Rapidly estimating natural gas compressibility factor. *J Nat Gas Chem* 16(4):349–353
- Bar-Meir G (2013) Fundamentals of compressible fluid\_mechanics Version 0.3.3.0. Chicago, p557
- Beggs DH, Brill JP (1973) A study of two-phase flow in inclined pipes. *J Pet Technol* 25(5):607–617
- Elizalde I, Ancheyta J (2015) Dynamic modeling and simulation of a naphtha catalytic reforming reactor. *Appl Math Model* 39(2):764–775
- Elsharkawy AM (2004) Efficient methods for calculations of compressibility, density and viscosity of natural gases. *Fluid Phase Equilibria* 218:1–13
- Fayazi A, Arabloo M, Mohammadi AH (2014) Efficient estimation of natural gas compressibility factor using a rigorous method. *J Nat Gas Sci Eng* 16:8–17
- George JA, Abdullah MA (2004) Catalytic naphtha reforming, 2nd edn. Marcel Dekker Inc., New York
- Heidaryan E, Moghadasi J, Rahimi M (2010) New correlations to predict natural gas viscosity and compressibility factor. *J Pet Sci Eng* 73(1–2):67–72
- Heidaryan E, Salarabadi A, Moghadasi J (2010) A novel correlation approach for prediction of natural gas compressibility factor. *J Nat Gas Chem* 19(2):189–192
- John YM, Patel R, Mujtaba IM (2018) Effects of compressibility factor on fluid catalytic cracking unit riser hydrodynamics. *Fuel* 223:230–251
- Kumar N (2004) Compressibility factors for natural and sour reservoir gases by correlations and cubic equations of state. Texas Tech University, Lubbock
- Li C, Peng Y, Dong J (2014) Prediction of compressibility factor for gas condensate under a wide range of pressure conditions based on a three-parameter cubic equation of state. *J Nat Gas Sci Eng* 20:380–395
- Mahmoud M (2014) Development of a new correlation of gas compressibility factor (Z-factor) for high pressure gas reservoirs. *J Energy Resour. Technol. Trans ASME* 136(1):012903–0129011
- Papay JA (1968) A termelestechnologiai Parameterek valtozasa a gastelepek muve-lesesoran. *OGIL Musz. Kuzl, Budapest: Tud*

18. Riazi M (2005) Characterization and properties of petroleum fractions, 1st edn. International Standards (ASTM), Philadelphia
19. Rodríguez MA, Ancheyta J (2011) Detailed description of kinetic and reactor modeling for naphtha catalytic reforming. *Fuel* 90(12):3492–3508
20. Sanjari E, Lay EN (2012) Estimation of natural gas compressibility factors using artificial neural network approach. *J Nat Gas Sci Eng* 9:220–226
21. Shokir EME-M, El-Awad MN, Al-Quraishi AA, Al-Mahdy OA (2012) Compressibility factor model of sweet, sour, and condensate gases using genetic programming. *Chem Eng Res Des* 90(6):785–792

**Publisher's Note** Springer Nature remains neutral with regard to jurisdictional claims in published maps and institutional affiliations.